THE JOURNAL OF BIOLOGICAL CHEMISTRY VOL. 283, NO. 52, pp. 36071–36087, December 26, 2008
Printed in the U.S.A.

Glutathione Depletion and Disruption of Intracellular Ionic Homeostasis Regulate Lymphoid Cell Apoptosis*

Received for publication, September 11, 2008, and in revised form, October 20, 2008 Published, JBC Papers in Press, October 21, 2008, DOI 10.1074/jbc.M807061200

Rodrigo Franco, Wayne I. DeHaven, Maria I. Sifre, Carl D. Bortner, and John A. Cidlowski[1]

From the Laboratory of Signal Transduction, NIEHS, National Institutes of Health, Research Triangle Park, North Carolina 27709

Intracellular glutathione (GSH) depletion is an important hallmark of apoptosis. We have recently shown that GSH depletion by its extrusion regulates apoptosis independently of excessive reactive oxygen species accumulation. However, the mechanisms by which GSH depletion regulates apoptosis are still unclear. Because disruption of intracellular ionic homeostasis, associated with apoptotic volume decrease (AVD), is necessary for the progression of apoptotic cell death, we sought to evaluate the relationship between GSH transport and ionic homeostasis during Fas ligand (FasL)-induced apoptosis in Jurkat cells. GSH depletion in response to FasL was paralleled by distinct degrees of AVD identified by differences in cellular forward scatter and electronic impedance analysis. Inhibition of GSH efflux prevented AVD, K^+ loss, and the activation of two distinct ionic conductances, mediated by Kv1.3 and outward rectifying Cl^- channels. Reciprocally, stimulation of GSH loss accelerated the loss of K^+, AVD, and consequently the progression of the execution phase of apoptosis. Although high extracellular K^+ inhibited FasL-induced apoptosis, GSH depletion was largely independent of K^+ loss. These results suggest that deregulation of GSH and ionic homeostasis converge in the regulation of apoptosis in lymphoid cells.

Apoptosis or programmed cell death is a ubiquitous energy-dependent, evolutionary conserved process. Under physiological conditions it is important not only in the constant turnover of cells in all tissues, but also during the normal development and senescence of the organism. Moreover, its deregulation has been observed to occur as either a cause or consequence of distinct pathologies (1, 2). A clear example is apoptosis mediated by Fas ligand (FasL)[2] receptor (Fas/CD95/Apo-1) activation, which is necessary for immune system homeostasis because of its role in the rapid clearance of immunoreactive T cells maintaining the immune balance and reducing the risk of autoimmune diseases (3). Apoptosis is a highly ordered process characterized by the progressive activation of precise pathways leading to specific biochemical and morphological alterations. Initial stages of apoptosis are characterized by activation of initiator caspases, changes in the cellular redox potential, intracellular ionic homeostasis, cell shrinkage or apoptotic volume decrease (AVD), loss of membrane lipid asymmetry, and chromatin condensation. Later stages associated with the execution phase of apoptosis are characterized by execution caspase and endonuclease activation, apoptotic body formation, and cell fragmentation (4, 5).

Reduced glutathione (GSH) is the most abundant low molecular weight thiol in animal cells and is the major determinant in the redox potential of the cell. It is involved in many cellular processes, including antioxidant defense, drug detoxification, signaling, and proliferation (6–10). Glutathione loss is an early hallmark in the progression of cell death in response to different apoptotic stimuli (11–19). Death receptor (including Fas)-induced GSH depletion has been clearly associated with the activation of a plasma membrane transport mechanism and not to its oxidation by reactive oxygen species (ROS) (20–23). Several studies have shown a correlation between GSH efflux and the progression of apoptosis, and inhibition of GSH loss is able to rescue cells from cell death progression (20–22). Glutathione depletion has been shown to directly modulate both the permeability transition pore formation and the activation of caspase 3 (24–26). In addition, *in vitro* studies have demonstrated that a reduction in the intracellular GSH content is necessary for the formation of the apoptosome (27). Additionally, high intracellular GSH (GSHi) levels have been associated with an apoptotic resistant phenotype (28–31). We and others have previously shown that FasL-induced GSH efflux is mediated by a transporter (22, 23, 32). Although GSH efflux precedes ROS formation (33, 34), we recently demonstrated that while GSH transport regulates apoptosis, neither GSH loss nor the progression of cell death are regulated by excessive and widespread formation of ROS or oxidative stress during apoptosis (34). However, the mechanism involved in the regulation of apoptosis by changes in GSHi are still elusive.

Apoptotic volume decrease (AVD) and changes in intracellular ionic homeostasis are common early features observed during apoptosis (5, 35–38). Although cell shrinkage or AVD is

* This work was supported, in whole or in part, by a National Institutes of Health grant (intramural research program of the NIEHS). The costs of publication of this article were defrayed in part by the payment of page charges. This article must therefore be hereby marked "*advertisement*" in accordance with 18 U.S.C. Section 1734 solely to indicate this fact.

[1] To whom correspondence should be addressed: Laboratory of Signal Transduction, NIEHS, National Institutes of Health, P. O. Box 12233, 111 TW Alexander Dr., Research Triangle Park, NC 27709. Tel.: 919-541-1564; Fax: 919-541-1367; E-mail: cidlows1@mail.nih.gov.

[2] The abbreviations used are: FasL, Fas ligand; AVD, apoptotic volume decrease; GSH_i, intracellular glutathione; K^+_i, intracellular potassium; ORCC, outward rectifying chloride channel; ROS, reactive oxygen species; FACS, fluorescence-activated cell sorting; DIC, differential interference contrast; FITC, fluorescein isothiocyanate; PBS, phosphate-buffered saline; PARP, poly(ADP-ribose) polymerase; PE, phycoerythrin; PI, propidium iodide; MRP, multidrug resistance protein; CV, cell volume; CD, cell diameter; DIDS, 4,4′-diisothiocyanostilbene-2,2′-disulfonic acid; BSO, DL-buthionine-(*SR*)-sulfoximine; ShK-Dap22, L-(α,β-diaminopropionyl[22])-*S. helianthus*; mBCl, monochlorobimane; PBFI-AM, 1,3-benzenedicarboxylic acid, 4,4′-[1,4,10,13-tetraoxa-7,16-diazacyclooctadecane-7,16-diylbis(5-methoxy-6,2-Benzofuran-diyl)]bis-tetrakis [(acetyloxy)methyl]ester.

an epi-phenomenon associated with ionic imbalance (39), changes in intracellular ion homeostasis during apoptosis have been shown to be necessary for the activation and assembly of the apoptotic machinery (5, 35–38). However, the exact signaling cascades that modulate the changes in ionic homeostasis have not been identified yet. Apoptotic volume decrease, changes in ionic homeostasis, and GSH loss have been observed to occur at early stages of apoptosis (5, 22). However, their interrelationship and further connection with the cell death program are unknown. Here we report that GSH efflux occurs concomitant to cell shrinkage or AVD and show that GSH transport is necessary for changes in intracellular ionic homeostasis, during FasL-induced apoptosis. Furthermore, we present evidence that the regulation of the execution phase of apoptosis by changes in GSH_i is mediated, at least in part, by the modulation of changes in the intracellular ionic balance.

EXPERIMENTAL PROCEDURES

Reagents—RPMI 1640 medium, penicillin/streptomycin, and heat-inactivated fetal calf serum were from Invitrogen. MK571 was from Biomol (Plymouth, PA). L-(α,β-Diaminopropionyl^{22})-*Stichodactyla helianthus* peptide neurotoxin (ShK-Dap22) was from Bachem (King of Prussia, PA). Monochlorobimane (mBCl) and 1,3-benzenedicarboxylic acid, 4,4′-[1,4,10,13-tetraoxa-7,16-diazacyclooctadecane-7,16-diyl-bis(5-methoxy-6,2-Benzofuran-diyl)]bis-tetrakis [(acetyloxy)-methyl]ester (PBFI-AM) were from Molecular Probes Inc. (Eugene, OR). Cytofix/cytoperm kit and monoclonal antibodies PE-conjugated anti-active caspase 3, and FITC-conjugated anti-PARP cleavage site were from BD Biosciences. Anti-caspase 3, anti-caspase 7, anti-PARP, and anti-α-fodrin antibodies (human-specific) were from Cell Signaling Technology Inc (Beverly, MA). All other reagents were from Sigma.

Cell Culture and Media—Jurkat cells, E6.1 clone (human leukemia) were obtained from American Tissue Culture Collection (Manassas, VA). Cells were cultured in RPMI 1640 medium containing 10% heat-inactivated fetal calf serum, 4 mM glutamine, 31 mg/liter penicillin, and 50 mg/liter streptomycin at 37 °C, 7% CO_2 atmosphere. Cells ($5–7 \times 10^5$ cells/ml) were incubated with Fas ligand (FasL) (Kamiya Biomedical Co. Seattle, WA) for the time indicated to induce apoptosis. In media containing high glutathione (+GSH) or high *S*-methyl-GSH, NaCl was substituted with 25 mM of each compound, maintaining the same osmolarity of the media. High extracellular K^+ medium (high $[K^+]_e$) was made by isosmolar substitution of extracellular 104 mM NaCl with KCl. Media osmolarity were measured on a Wescor 5500 vapor pressure osmometer (Logan, UT).

Fluorescence-activated Cell Sorting (FACS)—FasL-induced apoptotic parameters were analyzed by FACS, using an LSR II flow cytometer and FACSDiva software (BD Biosciences) for data analysis. Cells were analyzed at a cell density of $5–7 \times 10^5$ cells/ml, and 1×10^4 cells were recorded. Fluorophores were diluted in dimethyl sulfoxide (DMSO) and preloaded at 37 °C, 7% CO_2. The final concentration of DMSO never exceeded 0.1%. When indicated, propidium iodide (PI) was added to a final concentration of 10 μg/ml, to assess the loss of membrane integrity. Sequential analysis of the distinct fluorophores was used, and cells with increased PI fluorescence were excluded during the analysis. Cells were analyzed in FL-3 fluorescence for PI (488 nm excitation, 695/40 nm emission). Histograms and plots in all cases are representative of at least three different experiments. Changes in different morphological and biochemical parameters during apoptosis induced by FasL in Jurkat cells were determined as follows.

Changes in Forward Scatter (Cell Size)—Cell size was determined as changes in the forward scatter light pattern of the cells. Cells were excited with an argon 488 nm laser. The forward-angle light scatter relates to cell diameter, *i.e.* cell shrinkage is reflected as a decrease in the amount of forward scattered light.

Changes in Intracellular Glutathione Content, GSH_i—Cells were preloaded for 10 min with 10 μM mBCl, which forms blue fluorescent adducts with intracellular glutathione (40). Immediately prior to flow cytometry examination, PI was added. For mBCl, cells were excited with a UV 405 nm laser, and emission was acquired with a 440/40 filter. Changes in the GSH_i are reflected by the appearance of populations of cells with differences in mBCl fluorescence, reflecting changes in GSH_i. Populations were gated as described previously (22, 34). Briefly, contour plots of mBCl fluorescence *versus* forward scatter were used to identify populations of cells with different GSH_i levels induced after FasL treatment. Three different populations were identified and represented independently as follows: cells with high GSH_i or control cells (black); cells that displayed an initial reduction in GSH_i (10-fold decrease in mBCl fluorescence) and a slight decrease in their forward scatter properties (light gray); and cells with an enhanced depletion of GSH_i (100-fold decrease in mBCl fluorescence) and a marked decrease in forward scatter light (dark gray).

Changes in Intracellular Potassium, $K^+{}_i$—Cells were preloaded for 1 h with 5 μM PBFI-AM (K^+ fluorophore) prior to the time of analysis. The excitation peak of this benzofuran isophthalate derivative narrows significantly upon K^+ binding shifting the excitation maxima to shorter wavelengths and causing a large change in the ratio of energy absorbed at 340/380 nm. Immediately prior to flow cytometry examination PI was added. For PBFI, cells were excited with a UV 350/360 nm laser, and emission was examined with a 440/40 filter. Changes in the $K^+{}_i$ are reflected by the appearance of populations of cells with differences in PBFI fluorescence, reflecting changes in the intracellular concentration of this ion.

Analysis of Plasma Membrane Lipid Symmetry—Externalization of phosphatidylserine during apoptosis was determined by its binding to annexin V conjugated to FITC (Trevigen, Gaithersburg, MD). Briefly, control or treated cells, initially washed in PBS, were incubated with annexin-FITC and PI for 15 min at room temperature according to the manufacturer's instructions. Annexin-FITC/PI-stained samples were diluted in annexin binding buffer and examined immediately by FACS. FITC fluorescence was analyzed in FL-1 (488 nm excitation, 530/30 nm emission). Early apoptotic cells are defined as having annexin-positive, PI-negative staining. Late apoptotic and nonviable cells are both annexin- and PI-positive.

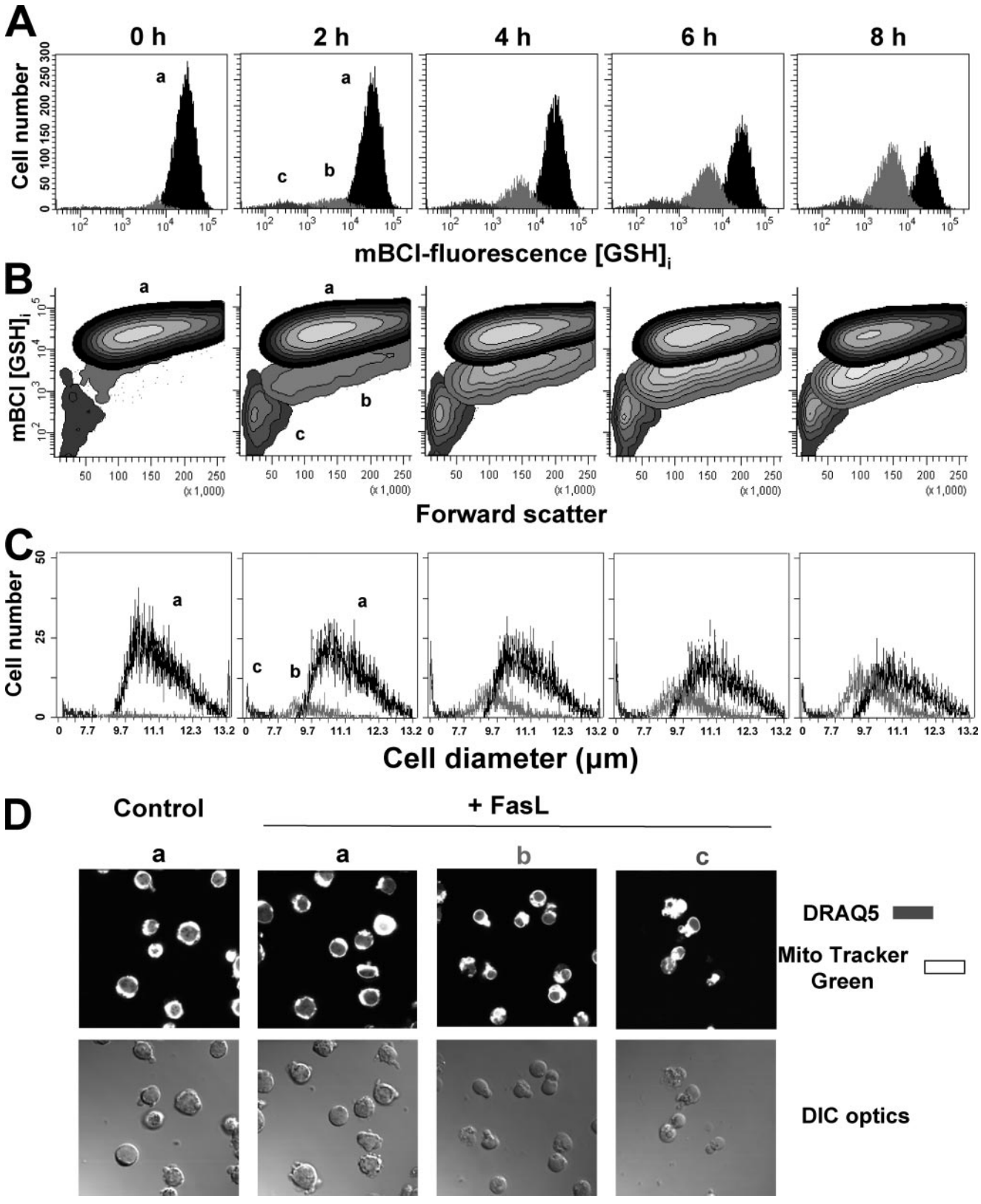

FIGURE 1. **Changes in GSH_i are paralleled by AVD or cell shrinkage.** Changes in GSH_i were determined by FACS using the thiol binding dye mBCl. For the induction of apoptosis, Jurkat cells were incubated with 25 ng/ml FasL for the time indicated. Data are expressed as frequency histograms of mBCl fluorescence (*A*) and contour plots of mBCl fluorescence *versus* changes in forward light scatter (*B*). Populations were gated according to their GSH_i levels on mBCl fluorescence *versus* forward scatter plot and represented as follows: normal cells with high GSH_i (*population a in black*) and cells with reduced GSH_i levels (*population b in light gray, and population c in gray*). *C,* changes in cell size of populations from *A* were analyzed by electronic impedance to determine cellular diameter as explained under "Experimental Procedures" and represented as in *A*. Plots and histograms are representative of at least four independent experiments. These populations were subsequently sorted for DIC optic imaging (*D*). Cells were prestained with DRAQ (for nuclear staining) and MitoTracker Green (for mitochondrial staining). Images are representative of three independent experiments.

TABLE 1

Changes in electronic cell diameter (CD), cell volume (CV), and cell number (% of total cell number) of populations with different levels of GSH_i induced by FasL

Data are means (X) ± S.E. of $n = 3$ independent experiments. Percentages in CV/CD columns for the first and second stages of GSH loss reflect the percentage of reduction with respect to normal high GSH values. Populations were gated from dot plots of mBCl fluorescence *versus* electronic CD and analyzed according to the levels of GSH; as in Fig. 1. CV is determined from the electronic cell diameter (d) and the sphere volume equation ($\pi \cdot d^3$)/6. Normal cells are cells with high GSH_i and normal cell size ~780 μm; cells within the first stage of GSH loss and AVD are cells with a 10-fold decrease in mBCl fluorescence and a decrease in cell size of ~17% (to ~650 μm); cells within the second stage of GSH loss and AVD are cells with a 100-fold decrease in mBCl fluorescence and a large decrease in cell size of ~95% (to ~39 μm); see control values.

	Populations with different levels of GSH_i								
	Normal high GSH_i population			1st stage of GSH_i loss			2nd stage of GSH_i loss		
	CD (μm)	CV (μm^3)	Cell number (%)	CD (μm)	CV (μm^3)	Cell number (%)	CD (μm)	CV (μm^3)	Cell number (%)
	X ± SE	X ± SE	X ± SE	X ± SE	X ± SE	X ± SE	X ± SE	X ± SE	X ± SE
Control	11.45 ± 0.05	786.12 ± 10.38	91.50 ± 1.50	10.77 ± 0.04 ** 6%	655.13 ± 8.76 ** 17%	2.03 ± 0.62	4.16 ± 0.21 ** 64%	38.68 ± 5.99 ** 95%	1.53 ± 0.18
Time dependence (10 ng/ml FasL)									
2 h	11.54 ± 0.11	804.66 ± 11.11	84.64 ± 5.71 *	10.62 ± 0.16 ** 8%	627.15 ± 15.16 ** 22%	10.43 ± 6.37 *	4.41 ± 0.36 ** 62%	44.90 ± 16.36 ** 94%	4.93 ± 0.45 *
4 h[a]	11.40 ± 0.05	775.85 ± 11.78	77.40 ± 2.63 *	10.46 ± 0.06 ** 8%	600.52 ± 11.54 ** 23%	16.97 ± 4.03 *	4.47 ± 0.25 ** 60%	47.69 ± 8.41 ** 94%	5.62 ± 1.52 *
6 h	11.51 ± 0.03	798.40 ± 6.74	70.47 ± 5.31 *	10.39 ± 0.09 ** 10%	587.28 ± 10.09 ** 26%	26.04 ± 3.94 *	4.48 ± 0.38 ** 61%	47.07 ± 14.38 ** 94%	3.49 ± 0.76 *
8 h	11.44 ± 0.10	783.92 ± 9.10	62.74 ± 3.05 *	10.23 ± 0.09 ** 11%	560.56 ± 10.09 ** 28%	33.25 ± 3.33 *	4.36 ± 0.58 ** 62%	43.39 ± 20.58 ** 94%	4.01 ± 1.11 *
Dose response (4 h)									
10 ng/ml FasL [a]	11.40 ± 0.05	775.85 ± 11.78	77.40 ± 2.63 *	10.46 ± 0.06 ** 8%	600.52 ± 11.54 ** 23%	16.97 ± 4.03 *	4.47 ± 0.25 ** 61%	47.69 ± 8.41 ** 94%	5.62 ± 1.52 *
25 ng/ml FasL	11.33 ± 0.03	762.24 ± 6.74	64.75 ± 5.73 *	10.30 ± 0.05 ** 9%	572.25 ± 9.62 ** 25%	33.09 ± 4.73 *	5.35 ± 0.21 ** 53%	50.97 ± 10.00 ** 93%	4.37 ± 1.70 *
50 ng/ml FasL	11.36 ± 0.05	768.98 ± 6.74	46.83 ± 3.75 *	10.23 ± 0.08 ** 10%	561.36 ± 14.57 ** 27%	48.42 ± 5.51 *	5.71 ± 0.32 ** 50%	59.67 ± 15.99 ** 92%	4.74 ± 0.91 *
100 ng/ml FasL	11.40 ± 0.05	775.85 ± 11.78	32.88 ± 4.13 *	10.33 ± 0.11 ** 9%	577.86 ± 11.11 26%**	62.04 ± 5.03 *	5.59 ± 0.36 ** 51%	53.81 ± 18.31 ** 93%	5.07 ± 1.85 *

* $p < 0.05$ against corresponding values for normal high GSH_i population.
** $p < 0.05$ against corresponding control values.
*** Values here are the same and repeated just for comparison.

Caspase 3 and PARP Cleavage Analysis—Cells were washed with phosphate-buffered saline (PBS) and then fixed and permeabilized using the Cytofix/Cytoperm kit for 30 min at room temperature in the dark according to the manufacturer's specifications. Cells were then pelleted and washed with the Perm/Wash buffer and stained with PE-conjugated anti-active caspase 3 or FITC-conjugated anti-PARP cleavage site-specific antibodies for 1 h at room temperature in the dark. Following incubation, cells were washed with the PermWash buffer and analyzed by flow cytometry. PE and FITC fluorescence were examined in FL-2 (488 nm excitation, 575/26 nm emission) and FL-1, respectively.

Electronic Cell Volume Determination—Jurkat cells, treated with or without 10 ng/ml FasL for 4 h, were incubated for an additional 10-min period with 10 μM mBCl. Cell volume (CV) measurements of normal and low mBCl fluorescence populations were performed by analysis of the electronic (impedance) Coulter volume with an NPE Quanta flow cytometer (NPE Systems, Pembroke Pines, FL) as described previously (41, 42). Electronic volume calibration was performed for each experiment with 6 μm UV excitable flow cytometry alignment beads (Align Flow, Molecular Probes). Monochlorobimane was excited with a 365-nm excitation filter, and emission was detected on a photomultiplier using a 450/55-nm filter. Populations were depicted in dot plots of mBCl fluorescence and cell diameter (CD) (not shown). Populations with different levels of mBCl fluorescence and hence different levels of intracellular GSH were analyzed in histograms according to their CD values. CV was determined from the electronic cell diameter (d) and the sphere volume equation ($\pi \cdot d^3$)/6.

Cell Sorting and Confocal Imaging of Cells with Different Intracellular Glutathione Concentration $[GSH]_i$—Jurkat cells, which had been treated with or without 10 ng/ml FasL for 4 h, were incubated for an additional 15-min period with 10 μM mBCl, 10 μM DRAQ (nuclear staining), and 150 nM Mito-Tracker Green (mitochondrial staining). Sorting of the normal and low mBCl fluorescent cells was accomplished using a BD Biosciences FACS Vantage SE flow cytometer. Sort gates were set on a forward-scatter *versus* mBCl fluorescence plot. Cells were then sorted based on their mBCl fluorescence and forward scatter properties (see Fig. 1*B*). Populations of cells with discrete fluorescence intensities, hence intracellular GSH levels, were immediately placed on coverslips and observed immediately using a Zeiss 510 UV laser scanning confocal microscope to obtain simultaneous DIC and confocal images. DRAQ was excited at 633 nm, and emission was col-

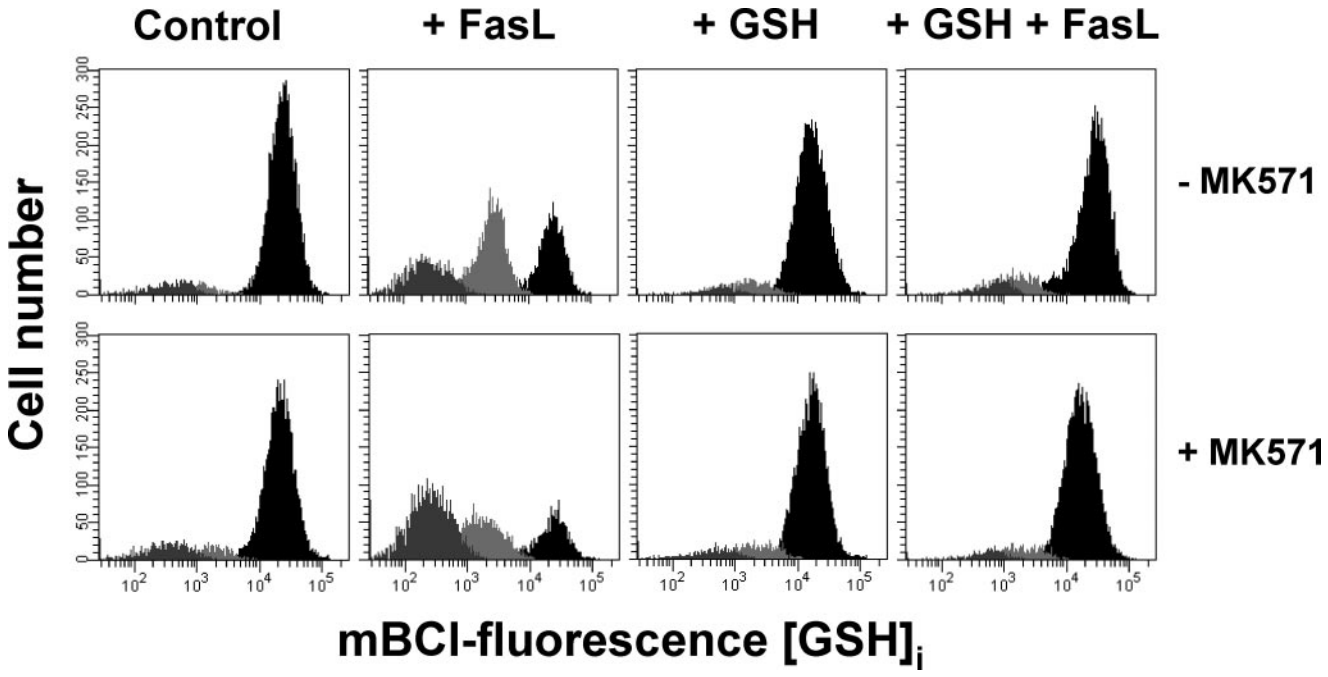

FIGURE 2. **Glutathione depletion is stimulated by MK571 and prevented by high extracellular GSH.** Intracellular GSH measurements by FACS were performed and represented as in Fig. 1*B*. Apoptosis was induced by 25 ng/ml FasL (4 h), in the presence or absence of 50 μM MK571 and high extracellular GSH medium (+*GSH*). High glutathione (+*GSH*) medium was made by substituting NaCl with 25 mM L-glutathione, maintaining the same osmolarity of the media. Plots are representative of at least four independent experiments.

lected with a 655–708-nm filter. MitoTracker Green was excited at 488 nm with an argon laser, and emission was collected with a BP 505–550-nm filter.

Differential Interference Contrast (DIC) Microscopy—A Zeiss LSM 510 microscope was used to obtain DIC images. Cells were pre-stained for 30 min at 37 °C and 5% CO_2 with 5 μg/ml Hoechst 33342 and then washed with fresh culture media. Hoechst-stained cells were examined with a Plan-Apo 63× oil N.A. = 1.4 objective lens to obtain simultaneous DIC and UV images. Hoechst was excited at 390 nm with a Titanium Saphire 750 nm laser, and emission was collected with a BP 465-nm filter. Images were analyzed with LSM 5 image browser software.

Protein Extraction and Western Immunoblotting—Cells were pelleted, washed once with ice-cold PBS, and lysed in buffer containing 20 mM Tris-HCl, 150 mM NaCl, 1 mM Na_2EDTA, 1 mM EGTA, 1% Triton X-100, and protease inhibitors (Complete Mini protease mixture, Roche Applied Science). Samples were sonicated and centrifuged, and the pellets were discarded. Then samples were assayed in a Beckman DU650 spectrophotometer for protein concentration using the Bio-Rad protein assay (Bio-Rad), and cell extracts were normalized to equal protein concentration. Loading buffer containing glycerol, SDS, and bromphenol blue was added, and samples were denatured at 99 °C for 5 min. Protein extracts, 50 μg/sample, were separated by SDS-PAGE on 4–20% gradient polyacrylamide Tris/glycine gels (Invitrogen) and transferred to nitrocellulose. Membranes were blocked in Tris-buffered saline containing 0.05% Tween, 10% nonfat dry milk, and 2% bovine serum albumin. Antibodies were diluted in Tris-buffered saline containing 0.05% Tween, 5% nonfat dry milk, and 1% bovine serum albumin. Blots were incubated with the corresponding primary antibody (1:1000) overnight. Then blots were incubated with the corresponding horseradish peroxidase-linked secondary antibodies (Amersham Biosciences) diluted 1:10,000. Blots were then visualized on film with the ECL chemiluminescent system (Amersham Biosciences). Blots were subsequently stripped using 65 mM Tris-HCl, pH 6.7, 100 mM β-mercaptoethanol, 2% SDS buffer and reprobed for α-tubulin (1:10,000) to verify equal protein loading.

Patch Clamp Electrophysiology—Whole-cell currents were investigated at room temperature (20–25 °C) in Jurkat cells using the patch clamp technique in the whole-cell configuration. Jurkat cells were bathed in HEPES-buffered saline solution containing (in mM) the following: 140 NaCl, 5 KCl, 2.2 $CaCl_2$, 1 $MgCl_2$, 10 HEPES, and 10 glucose at pH 7.3–7.4 (with NaOH), and voltage-clamped to −80 mV with an Axopatch 200B amplifier (Axon Instruments, Foster City, CA). Fire-polished pipettes fabricated from borosilicate glass capillaries (WPI, Sarasota, FL) with 5–7-megohm resistance were filled with pipette solution containing (mM) 140 potassium aspartate, 2.2 $CaCl_2$, 1 $MgCl_2$, 10 1,2-bis(*o*-aminophenoxy)ethane-*N*,*N*,*N*′,*N*′-tetraacetic acid, 10 HEPES, and 5 MgATP at pH 7.1–7.2 (with KOH). The reference electrode was a AgCl-wired pellet. Cells were treated with FasL in cell culture medium at 37 °C, 7% CO_2. Immediately prior to recording Jurkat cells were gently washed and resuspended in bath solution. Potassium and/or chloride (Cl^-) currents were evoked by a range of 100-ms voltage steps from −60 to +60 mV from a holding potential of −80 mV. The currents were measured after 1 min of attaining the whole-cell configuration. Cell capacitance obtained through the pCLAMP software was between 3 and 5 picofarads. Access resistance was typically between 10 and 30 megohms. Data were digitized at 2.5 kHz and filtered at 2 kHz. The currents were acquired

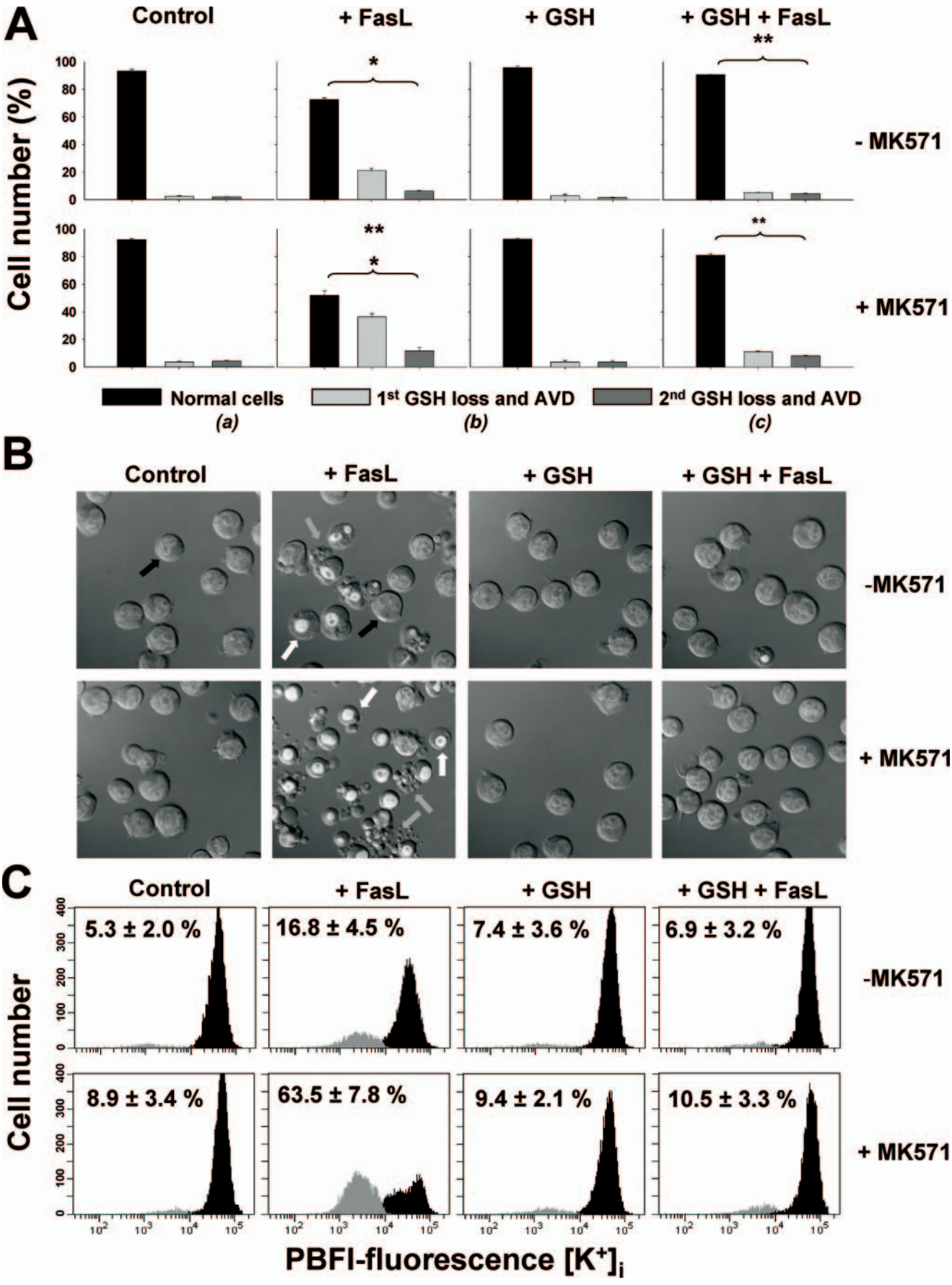
A
Control
+ FasL
+ GSH
+ GSH + FasL
Cell number (%)
- MK571
+ MK571
Normal cells
1st GSH loss and AVD
2nd GSH loss and AVD
(a)
(b)
(c)
B
Control
+ FasL
+ GSH
+ GSH + FasL
-MK571
+ MK571
C
Control
+ FasL
+ GSH
+ GSH + FasL
Cell number
5.3 ± 2.0 %
16.8 ± 4.5 %
7.4 ± 3.6 %
6.9 ± 3.2 %
8.9 ± 3.4 %
63.5 ± 7.8 %
9.4 ± 2.1 %
10.5 ± 3.3 %
-MK571
+ MK571
PBFI-fluorescence [K+]i

with pCLAMP-9 and analyzed with Clampfit 9.2 (Axon Instruments).

Statistical Analysis—When indicated, significance of differences in mean values was calculated using the two-tailed Student's *t* test. The number of experiments performed is indicated in the corresponding legend of the figures.

RESULTS

FasL-induced Reduction in Intracellular GSH Content (GSH_i) Is Paralleled by Apoptotic Volume Decrease (AVD)—Glutathione depletion and AVD are common early hallmarks of apoptosis induced by numerous stimuli (5, 8, 14, 43). We recently reported that GSH loss induced by FasL is mediated through the activation of an efflux transport mechanism for GSH extrusion rather than due to its oxidation to GSSG or loss of membrane integrity (22, 23, 34). Thus, we sought to investigate the relationship between AVD and GSH depletion during apoptosis. We first analyzed if GSH loss was associated with cell shrinkage or AVD. Single cell analysis of changes in GSH_i was done using FACS and the GSH binding dye mBCl. We have previously reported that GSH loss occurs stochastically reflected by the appearance of discrete populations with changes in GSH_i. These populations represent two different stages of GSH loss (22, 34). Fig. 1 shows that cells stained with mBCl show a high level of fluorescence depicted as a single population of cells, which reflects the basal levels of GSH_i (Fig. 1*A*, *0 h panel*). Fas ligand induced a progressive reduction in the population of cells with normal GSH_i content (Fig. 1*A*, *population a, depicted in black*). Additionally, FasL induced the appearance of two populations of cells with different levels of decreased GSH_i. A progressive increase in the population of cells within the first stage of depleted GSH_i (Fig. 1*A*, *population b, depicted in light gray*) and the proportional decrease in cells with high GSH_i were observed over time after Fas stimulation. In contrast, the population of cells within the second stage of GSH_i loss (Fig. 1*A*, *population c depicted in dark gray*) does not increase over time, which suggests that this stage is likely to be associated with the degradation phase of apoptosis, although these cells have integral plasma membrane observed as PI exclusion (not shown).

We have previously shown that AVD occurs in stages (41, 42). To analyze if GSH loss is paralleled by AVD, changes in GSH_i and in forward scatter properties were simultaneously analyzed. Forward-angle light scatter of cells relates to its diameter (44). Contour plots of mBCl fluorescence *versus* forward scatter (Fig. 1*B*) show that the distinct populations of GSH loss are distinguished by their differences in their forward scatter properties. The first population of cells with reduced GSH_i shows a slight decrease in forward scatter (Fig. 1*B*, *population b*), although the second population of cells has a marked decrease in forward scatter (*population c*). To test the validity of these observations via a different approach, we analyzed changes in cell volume using electronic (impedance) Coulter cell size determinations (cell diameter and cell volume) of each population of cells with different levels of GSH_i. Histogram analysis of the cell diameter for these populations shows that the two stages of GSH_i loss (Fig. 1*C*, *populations b and c*) are paralleled by distinct degrees of cell shrinkage reflected as a reduction in the mean electronic cell diameter (CD) of each population.

A nonlinear relationship exists between CD and cell volume (CV), which means that a small change in CD reflects a profound change in CV. Table 1 summarizes the results regarding the changes in CD and CV of each population in response to FasL. The normal population of cells with high GSH_i has a mean CD of ~11.4 μm and a mean CV of ~780 μm. The first population of cells within the first stage of GSH loss had a small but significant reduction in their mean EV of ~8–11% compared with control cells, which translates to a reduction in their mean CV of ~17–28%. Finally, the second population of cells within a large reduction in GSH_i showed a decrease in CD of ~50–62% compared with control cells and an enhanced decrease in CV of ~92–94% compared with control cells. These changes in the mean CD and CV values for each population (*i.e.* percentage of CD/CV reduction compared with the normal population of cells) were not significantly altered either by increasing concentrations of FasL or by the time of the treatment. However, the number of cells within the high GSH_i population was reduced in a dose- and time-dependent manner after FasL treatment, while the number of cells within the first population of GSH loss was proportionally increased (Fig. 1*C* and Table 1). The number of cells within the second population, which showed a large depletion in GSH_i and cell shrinkage significantly increased in response to FasL (from 1.5 to ~4%). However, this population did not respond to increasing concentrations of the ligand or to longer periods of exposure. This observation is consistent with the idea that this population is in constant demise and thus in the degradation phase of apoptosis (see Fig. 1*C* and Table 1). It is important to note that these populations were still detected at low levels in control cells in the absence of FasL, most likely reflecting the spontaneous apo-

FIGURE 3. **Intracellular GSH loss is necessary for cell shrinkage or AVD and K^+ loss.** Apoptosis was induced by 25 ng/ml FasL (4 h) in the presence or absence of 50 μM MK571 with or without high extracellular GSH medium (*+GSH*). Changes in electronic cell volume and GSH_i levels (*A*) were simultaneous analyzed as explained under "Experimental Procedures." *A, bar graphs* show the changes in the number of cells for each population with different levels of GSH_i and AVD represented as follows: *a,* normal cells with high GSH_i and a cell size of ~760 μm (*black*); *b,* cells within the first stage of GSH loss and a mean cell size of ~570 μm (*light gray*); and *c,* cells within the second stage of GSH loss and mean cell size of ~51 μm (*gray*). (See Table 1, values at 4 h of exposure to 25 ng/ml FasL.) Data are means ± S.E. of $n = 3$. *, $p < 0.005$ against control values for each population; **, $p < 0.005$ against FasL values for each population. *B,* cells were pre-stained with Hoechst 33342 and then washed with fresh culture media. Differential interference contrast microscopy was used to analyze changes in cell morphology during apoptosis. As shown in Fig. 1*C*, cells with a slight decrease in cell volume and condensed nuclei (*light gray arrows*), correspond to the first stage of GSH loss. Cells in later stages of apoptosis, characterized by plasma membrane blebbing and cell fragmentation, are associated with the second stage of GSH depletion (*gray arrows*). Control cells are characterized by a big nuclei and normal cell size (*black arrows*). Images are representative of at least three independent experiments. *C,* changes in the intracellular K^+ content were assessed using the K^+ fluorophore PBFI-AM. Frequency histograms of PBFI fluorescence show the appearance of a population of cells with a reduction in K^+_i (*gray*) upon Fas stimulation, compared with control cells (*black*). % are means ± S.E. of four independent experiments and represent the population of cells with a reduction in K^+_i. Plots are representative of at least four independent experiments.

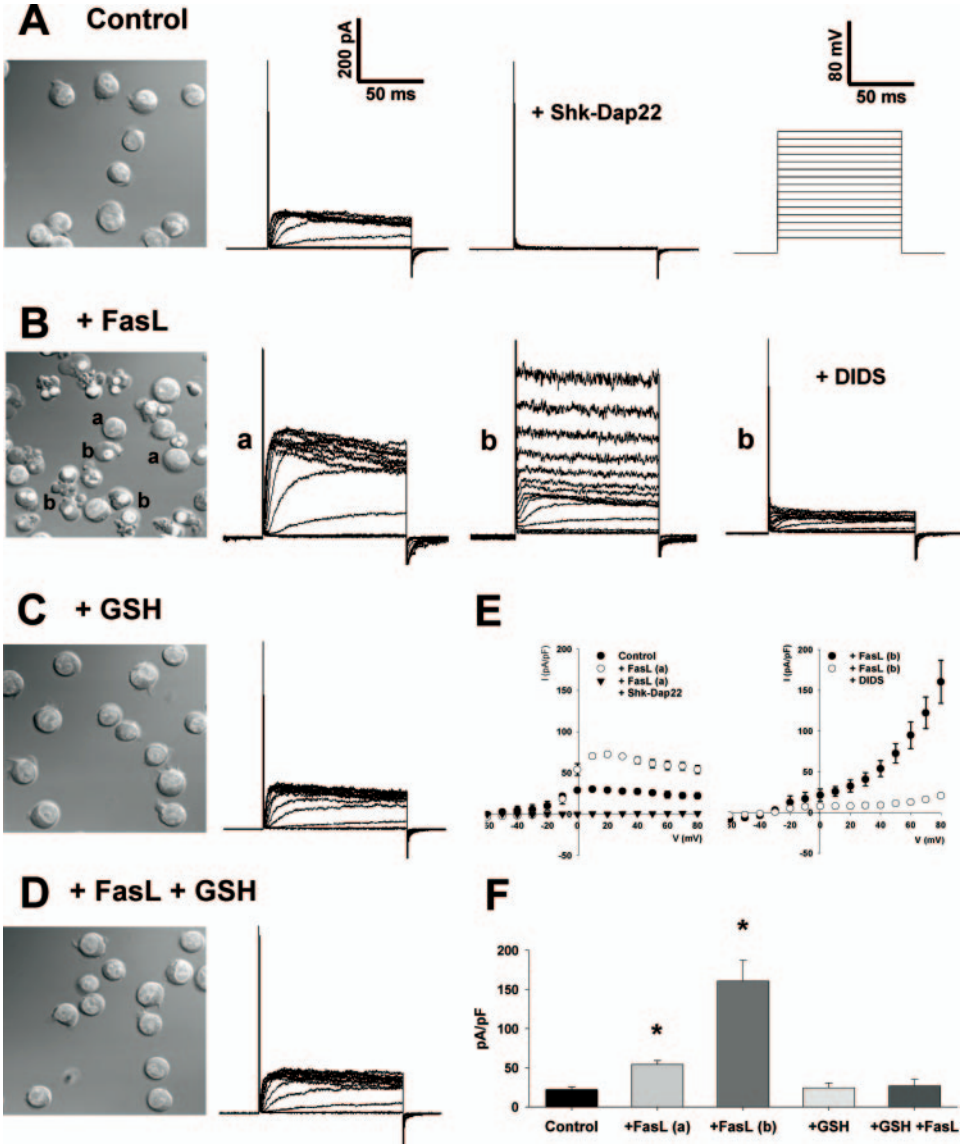

FIGURE 4. **FasL-induced activation of Kv1.3 and ORCC are modulated by changes in intracellular GSH.** Apoptosis was induced by 2 μg/ml FasL (1 h) in the presence or absence of high extracellular GSH medium (+*GSH*). DIC microscopy images in *A–D* were obtained as described previously to represent the population of cells that were subject to electrophysiology characterization. Activation of the ion channels Kv1.3 and ORCC was assessed by the patch clamp technique in its whole-cell configuration. *A,* representative plot of K^+ currents evoked in control untreated Jurkat cells is shown. These currents were blocked in the presence of 20 nM Shk-Dap22, which suggests that they are mediated by the voltage-gated channel Kv1.3. The *scale* in *A* applies to all subsequent current plots. Currents were evoked from a range of test potentials from −60 to 80 mV for 100 ms, from a holding potential of −80mV (see the voltage protocol in the *right inset* in *A*). FasL treatment of Jurkat cells induces the appearance of distinct populations of cells characterized by different morphological features (*B*), whose ion currents were characterized. In 36% of *a*-labeled cells (11 of 31 recordings), which observed normal morphological characteristics, an increase in the amplitude of voltage-activated Kv1.3-mediated K^+ currents was detected. This increase was completely inhibited in the presence of Shk-Dap22 (see *E*). A second population of cells (*b*), which observe common morphological features of apoptosis, including nuclei condensation, cell shrinkage, and plasma membrane blebs, showed the activation of an ORCC inhibited by 320 μM DIDS (see also *E*). In the presence of high extracellular GSH (*C* and *D*), which prevents the progression of apoptosis, Jurkat cells present basal levels of voltage-activated K^+ currents (as in *A*). *E*, current (*I*)-voltage (*V*) relationships of currents observed in *A* and *B* are shown. The current measured after 50 ms of test pulse and normalized for cell capacitance was plotted against the test potential. *F*, current elicited by an 80-mV test pulse from a −60-mV holding potential was measured after 50 ms recording and normalized by cell capacitance. FasL-induced increase in Kv1.3 (*a*) and ORCC (*b*) currents is prevented in the presence of high GSH medium. Plots are in all cases representatives of at least six independent recordings, and data in *E* and *F* are means ± S.E. of at least six independent experiments. *, $p < 0.005$ against control current values.

ptosis of the Jurkat cell population. Thus, these results demonstrate that FasL-induced GSH loss is associated with the different stages of cell shrinkage or AVD.

To evaluate the morphological features of these populations, cells were sorted, and then DIC and fluorescent images were simultaneously acquired (Fig. 1*D*). Control cells (Fig. 1*D, panel a*) showed normal morphology characterized by a large nuclei surrounded by mitochondria. Similar characteristics were observed for the population of cells with normal GSH_i after FasL treatment (Fig. 1*D, panel a* in FasL). The first population of cells with depleted GSH_i showed a reduction in cell size and nuclear condensation (Fig. 1*D, panels b*). The second population (Fig. 1*D* , *panels c*) showed a high degree of membrane blebbing and cell fragmentation that correlates with a marked reduction in their forward scatter properties. These data support the hypothesis that these cells are in the degradation or execution phase of apoptosis. Thus, FasL-induced GSH efflux occurs in two stages, reflected as the appearance of two different populations of cells with different GSH_i levels, which may represent different stages during apoptosis.

Glutathione Transport Regulates AVD during FasL-induced Apoptosis—We previously showed that GSH loss during FasL-induced apoptosis is stimulated by the presence of a wide variety of structurally unrelated agents (taurocholic acid, estrone sulfate, probenecid, and MK571) and inhibited by high extracellular GSH concentrations (22, 34). It was shown that MK571 is a potent stimulator of FasL-induced GSH efflux in Jurkat cells, and thus GSH loss (22). Fig. 2 shows that FasL-induced GSH loss is stimulated by MK571 and inhibited by high GSH medium. These results have been previously corroborated by analyzing the accumulation of extracellular GSH (in its reduced form) induced by FasL, which is also stimulated by MK571 (22, 34).

We next evaluated the relationship between GSH transport and AVD by analyzing the effects of MK571 and high GSH medium on cell shrinkage. Apoptotic volume decrease during FasL-induced apoptosis is a stochastic phenomenon. As demonstrated above, FasL induces a decrease

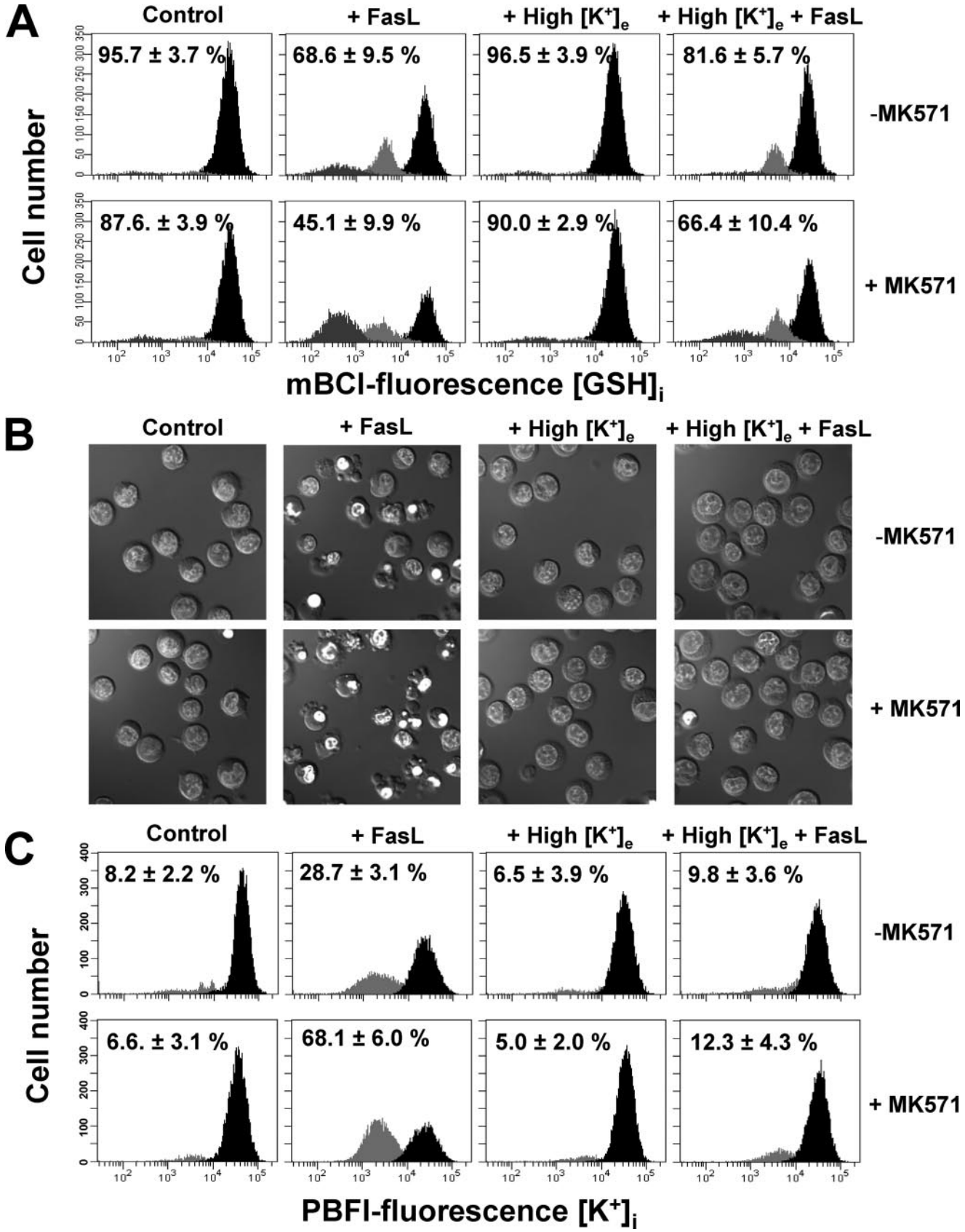

FIGURE 5. **K^+ loss is necessary for apoptosis but not for GSH loss.** Apoptosis was induced by 25 ng/ml FasL (4 h) in the presence or absence of 50 μM MK571 and high extracellular K^+ medium (*High* $[K^+]_e$). High $[K^+]_e$ was made by isosmolar substitution of extracellular NaCl with KCl. Changes in GSH_i (*A*), DIC optics (*B*), and K^+_i (*C*) were determined as described previously. Plots are representative of $n = 4$ independent experiments, and the % are means ± S.E. representing the population of cells with high GSH_i (*A*) or reduced K^+_i content (*C*). Images are representative of at least three independent experiments.

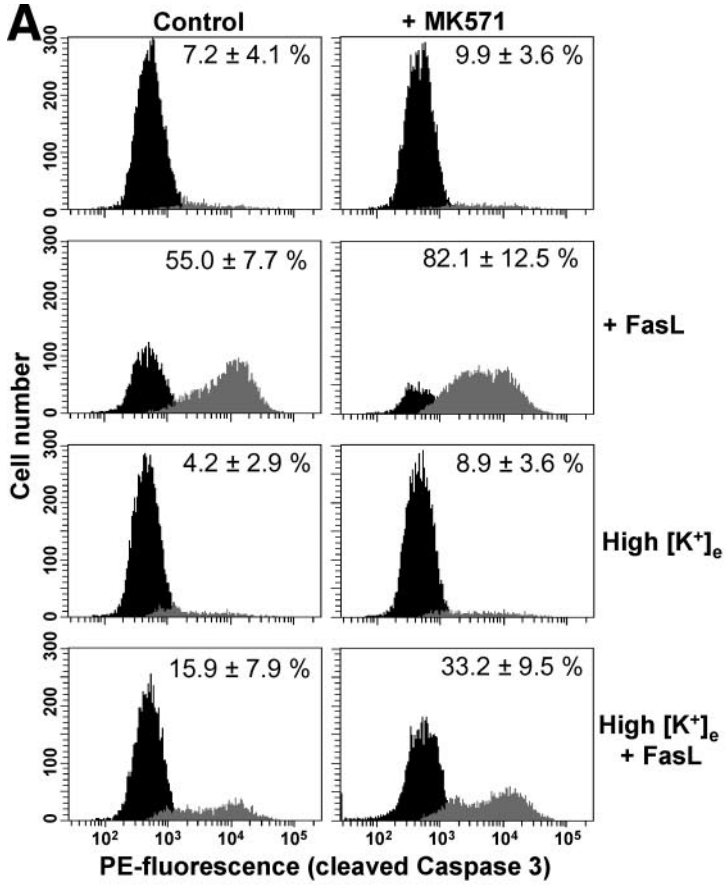
A
Control
+ MK571
7.2 ± 4.1 %
9.9 ± 3.6 %
55.0 ± 7.7 %
82.1 ± 12.5 %
+ FasL
4.2 ± 2.9 %
8.9 ± 3.6 %
High [K+]e
15.9 ± 7.9 %
33.2 ± 9.5 %
High [K+]e + FasL
Cell number
PE-fluorescence (cleaved Caspase 3)

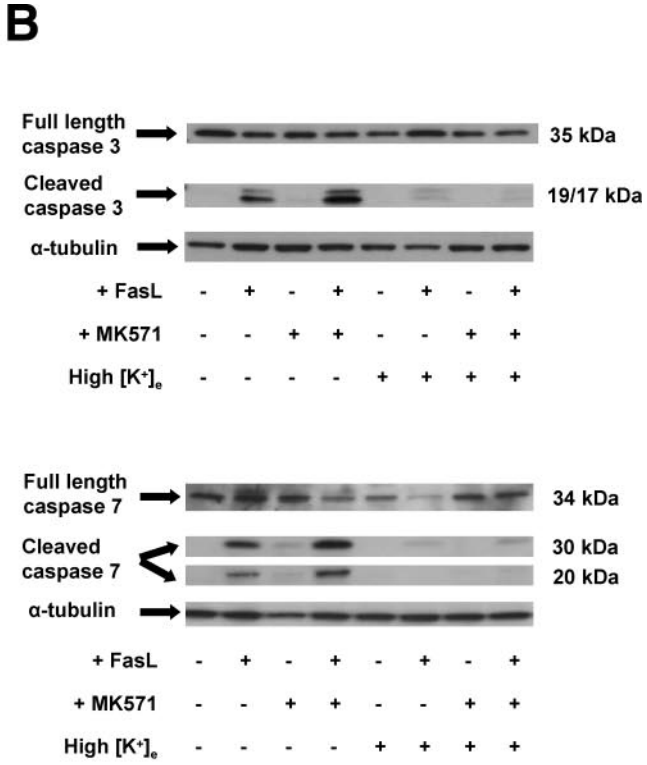
B
Full length caspase 3
35 kDa
Cleaved caspase 3
19/17 kDa
α-tubulin
+ FasL
+ MK571
High [K+]e
Full length caspase 7
34 kDa
Cleaved caspase 7
30 kDa
20 kDa
α-tubulin
+ FasL
+ MK571
High [K+]e

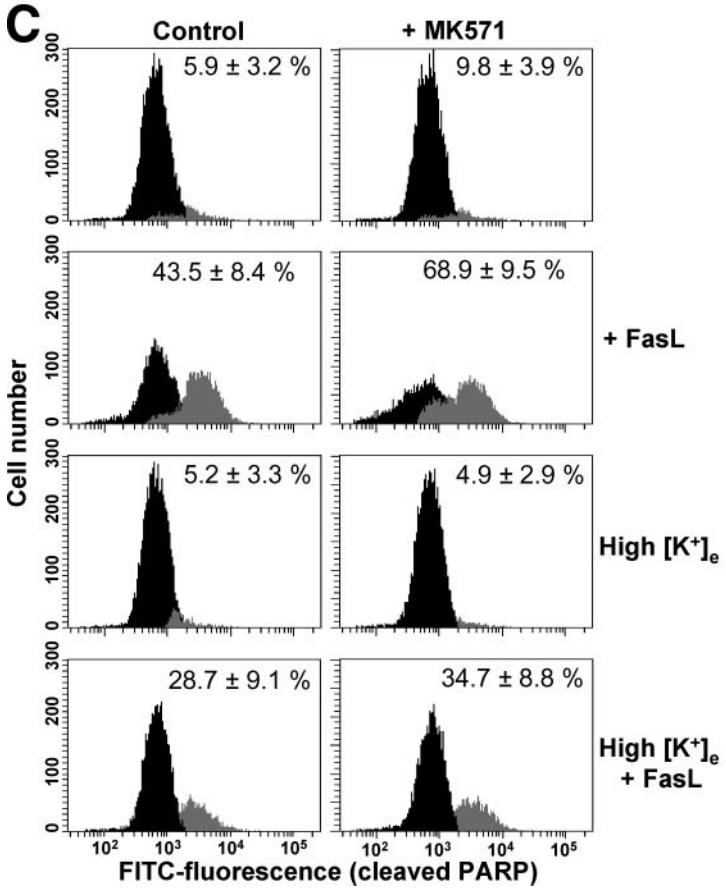
C
Control
+ MK571
5.9 ± 3.2 %
9.8 ± 3.9 %
43.5 ± 8.4 %
68.9 ± 9.5 %
+ FasL
5.2 ± 3.3 %
4.9 ± 2.9 %
High [K+]e
28.7 ± 9.1 %
34.7 ± 8.8 %
High [K+]e + FasL
Cell number
FITC-fluorescence (cleaved PARP)

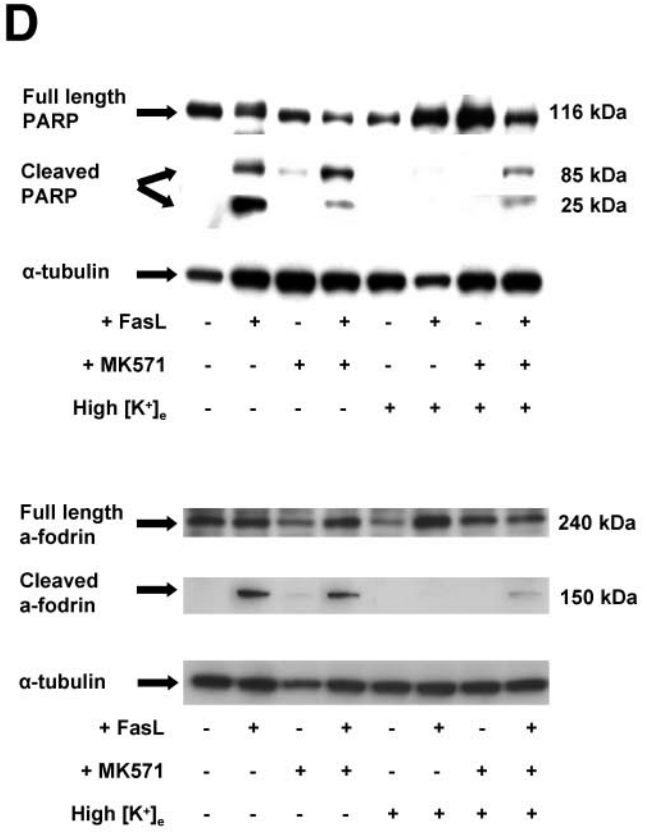
D
Full length PARP
116 kDa
Cleaved PARP
85 kDa
25 kDa
α-tubulin
+ FasL
+ MK571
High [K+]e
Full length a-fodrin
240 kDa
Cleaved a-fodrin
150 kDa
α-tubulin
+ FasL
+ MK571
High [K+]e

in the population of cells with high GSH_i and a proportional increase in the population of cells with decreased GSH_i; however, the mean CV for these populations remains constant, independent of the time of exposure and concentration used of FasL (see Fig. 1*C* and Table 1). This suggests that cell shrinkage occurs in stages very well defined by distinct populations, and thus the effects of MK571 and high GSH were evaluated on the number of cells for each population cells at different stages of AVD. Fig. 3*A* shows that MK571 increases the number of cells within the first population which observe depleted GSH_i and a small decrease in cell size after Fas activation (~570 μm, see Table 1, values at 4 h of exposure to 25 ng/ml FasL). This change occurred in parallel with a decrease in the population of cells with high GSH_i and normal cell size (~760 μm). In addition, MK571 increased the number of cells within the second population of GSH_i depletion that have a marked degree of cell shrinkage (~51 μm). High concentrations of extracellular GSH prevented the increase in the number of cells at both stages of GSH loss and AVD induced by FasL in the presence or absence of MK571. These data demonstrate that GSH transport modulates the progression of AVD.

We also investigated the role of GSH in the regulation of AVD and apoptosis by DIC microscopy imaging. Fig. 3*B* shows that FasL-induced apoptosis in Jurkat cells is characterized by cells at initial stages of apoptosis, with a small decrease in cell size and condensed nuclei (*white arrows*), which correspond to cells within the first stage of GSH loss (see Fig. 1*D*). Cells at later stages of apoptosis are characterized by a high degree of plasma membrane blebbing and cell fragmentation (Fig. 3*B, gray arrows*) that correspond to the cells within the secondary stage of GSH depletion (see Fig. 1*D*). Addition of MK571 stimulated cell shrinkage, membrane blebbing, and cell fragmentation, which were completely prevented by high extracellular GSH (+GSH) medium.

FasL-induced GSH Loss Regulates Changes in Intracellular Ionic Homeostasis upon FasL Stimulation—Apoptotic volume decrease has been reported to be a consequence of the disruption of intracellular ionic homeostasis (5, 43). Alterations in ionic gradient distribution during apoptotic cell death have been shown to be the result of both impaired ionic homeostatic mechanisms (ATPases) and activation of ion flux pathways (channels) (36, 45–47). Changes in cellular ionic homeostasis during apoptosis are not only initial hallmarks of this phenomenon but also important regulators of the progression of apoptosis by the modulation of the apoptotic signaling machinery (5, 35–38). It is well known that apoptosis induced by different stimuli leads to a loss of K^+_i that is necessary for AVD and the progression of apoptosis (5, 45, 48–50). Because FasL-induced GSH transport modulates AVD, we next investigated if GSH transport modulates changes in intracellular ionic homeostasis during apoptosis. We first investigated if changes in K^+_i were also modulated by GSH transport using the K^+-binding fluorescent indicator PBFI-AM. Fig. 3*C* shows that FasL induces the appearance of a population of cells with a reduction in K^+_i (to 17%, *gray population*) compared with control cells (*black population*). This population was augmented by the presence of MK571 (to 64%). High extracellular GSH prevented K^+_i loss induced by FasL and its stimulation by MK571.

Activation of apoptosis by a variety of stimuli, including FasL, has also been reported to induce the activation of distinct ionic conductances (5, 35, 37), including voltage-gated K^+ channels (such as Kv1.3) and outward rectifying chloride channels (ORCC) (37, 51, 52). We analyzed if GSH transport regulated the activation of these ionic conductances by FasL. Fig. 4 shows representative whole-cell currents elicited from control untreated cells by voltage step depolarizations. These currents correspond to the activation of the voltage-gated K^+ channel Kv1.3 as evidenced by its complete inhibition in the presence of the monosubstituted analog of the sea anemone toxin Shk-Dap22. Kv1.3 has been proposed to be the predominant voltage-gated K^+ channel in Jurkat cells (51, 53); however, it is possible that Shk-Dap22 might also inhibit other voltage-gated K^+ channels (54, 55).

Apoptosis is a stochastic phenomenon characterized by its asynchronized progression that conveys the appearance of distinct populations of cells at different stages of the cell death process. Fig. 4*B* shows that FasL induces the appearance of cells with different morphological characteristics as explained in Figs. 1*D* and 3*B*. These populations were characterized by means of patch clamp electrophysiology. In ~36% of the population of cells with normal morphology (11 of 31 recordings of *a*-labeled cells), an increase in the voltage-activated K^+ current amplitude, which is completely inhibited in the presence of Shk-Dap22 (Fig. 4, *B*, *a,* labeled cells, and Fig. *E*), was observed. In a second population of cells characterized by a smaller size, condensed nuclei, and in some cases, plasma membrane blebbing (Fig. 4*B*, *b,* labeled cells), we detected the activation of the ORCC as evidenced by its inhibition in the presence of DIDS (37, 56). DIDS-induced inhibition of ORCC evidenced a reduction in the voltage-dependent K^+ currents, which has been demonstrated to occur during late stages of apoptosis (57, 58). Interestingly, a recent report shows that a surge in Cl^- conductances is actually associated with impaired Kv1.3 activity (59). High extracellular GSH completely prevented the activation of these conductances by FasL (Fig. 4, *C–F*). These results suggest that GSH depletion modulates the activation of ionic conductances during apoptosis.

FIGURE 6. **GSH depletion modulates the execution phase of apoptosis by regulation of K^+ loss.** Apoptosis was induced by 25 ng/ml FasL during 4 h in the presence or absence of 50 μM MK571 and high extracellular K^+ medium (High $[K^+]_e$). The execution phase of apoptosis was evaluated by the activation of execution caspases (3 and 7) and cleavage of their substrates (PARP and α–fodrin). *A* and *C,* immunolabeling detection of cleaved caspase 3 and PARP was performed by single cell analysis using FACS. Frequency histograms in control panels show the distribution of cells with background fluorescence for PE-conjugated anti-active caspase 3 or FITC-conjugated anti-cleaved PARP antibodies (*black*). A second population with increased fluorescence for PE or FITC (*gray*) indicates the cells with activated/cleaved caspase 3 (*A*) and PARP (*C*), respectively. Plots are representative of at least four independent experiments, and the percentages are means ± S.E. representing the population of cells with active caspase 3 (*A*) or cleaved PARP (*C*). *B* and *D*, Western immunoblot analysis was done on whole-cell lysates of experimental samples, and blots were incubated with the corresponding antibodies as explained under "Experimental Procedures." Blots were stripped and reprobed for α-tubulin to verify equal protein loading and are representative of at least three independent experiments.

GSH Regulates the Execution Phase of Apoptosis by the Modulation of K^+_i Loss—We recently reported that GSH efflux is necessary for the progression of the execution phase of apoptosis (22) and that this is independent from the excessive generation of ROS (34). However, the exact mechanism by which the reduction in GSH_i modulates the activation of the execution phase of apoptosis is still imprecise. A necessary role of K^+ loss for the activation of execution caspases and apoptosome formation has also been demonstrated (5, 60, 61), whereas Cl^- loss does not seem to play an important role in this phenomenon (62). Thus, we analyzed if the modulation of the execution phase of apoptosis by GSH transport was linked to the regulation of K^+ loss. Potassium loss during apoptosis has been reported to be mediated by its passive transport across the membrane driven by its electrochemical gradient; hence, it has been ascribed to the activation of K^+ channels. Accordingly, we evaluated the effects of high extracellular K^+ conditions, which have been shown to inhibit K^+ loss during apoptosis (63), on the changes in GSH_i induced by FasL. Glutathione loss was shown to be largely unaffected by high K^+ conditions (Fig. 5*A*). However, high K^+ was still able to prevent not only AVD but also plasma membrane blebbing, nuclei condensation (Fig. 5*B*), as well as K^+ loss (Fig. 5*C*) during FasL-induced apoptosis. In addition, high K^+ medium blocked the stimulatory effects of MK571 on the progression of the execution phase of apoptosis (Fig. 5, *B* and *C*). Fig. 6 shows that high K^+ medium inhibits the cleavage of execution caspases 3 and 7 as well as that of their substrates PARP and α-fodrin. Furthermore, it also inhibited the stimulatory effects of MK571, which accelerates GSH transport, on the cleavage of these proteins. Together, these results suggest that GSH loss occurs prior to, and independent of, K^+ efflux during apoptosis. Potassium loss however is still necessary for the progression of apoptosis. Thus GSH efflux is coupled to AVD and changes in ionic homeostasis. Moreover, GSH transport seems to modulate the progression of the execution phase of apoptosis by regulation of K^+ loss.

Regulatory Effect of GSH on Apoptosis Depends on the –SH (Thiol) Group—The cysteinyl moiety of GSH provides the reactive thiol group (–SH group) that allows GSH to participate in a wide variety of metabolic processes, including oxidation-reduction (redox) reactions and nucleophilic displacement or addition-type reactions (6, 64). We have previously demonstrated that excessive ROS formation and widespread oxidative stress during FasL-induced apoptosis do not regulate the progression of cell death (34). To elucidate if the regulatory role of GSH in apoptosis depends on its thiol group, we studied the effects of the modified analog *S*-methyl-GSH on apoptosis. Fig. 7*A* shows that FasL-induced apoptosis, assessed by the externalization of phosphatidylserine (annexin V) and changes in the plasma membrane integrity of the cell (PI uptake), was suppressed by high extracellular GSH. In contrast, *S*-methyl-GSH prevented neither apoptosis (Fig. 7*B*) nor the activation of ionic conductances by FasL (Fig. 7*C*), which suggests that the regulatory role of GSH in apoptosis is dependent on its thiol moiety.

GSH Depletion Triggers Apoptosis in the Absence of Apoptotic Stimuli—We have demonstrated that inhibition of the γ-glutamylcysteine synthetase by BSO for 24 h depletes GSH from Jurkat cells (22). Under these conditions, depletion of GSH_i with BSO stimulated apoptosis induced by submaximal concentrations of FasL (Fig. 8*A*). Apoptosis induces both GSH extrusion (20–23, 32, 33, 65) and inhibition of its synthesis by caspase-mediated cleavage of the γ-glutamylcysteine synthetase (66, 67). Glutathione depletion by itself has been observed to either induce or stimulate apoptosis. In particular, BSO-induced GSH depletion does not trigger apoptosis but potentiates death receptor-induced apoptosis in T cells (28, 31, 68–70). As shown in Fig. 8*A*, inhibition of GSH synthesis by BSO potentiates apoptosis induced by FasL in Jurkat cells. Although GSH depletion induced by BSO does not seem to be sufficient to induce apoptosis in the absence of apoptotic stimuli, addition of MK571 to GSH-depleted cells induces cell death with characteristics of apoptosis (Fig. 8, *B* and *C*). Cells treated with both BSO and MK571 observed initial externalization of phosphatidylserine, secondary loss of plasma membrane integrity (Fig. 8*B*), nuclei condensation, plasma membrane blebbing, and cell shrinkage (Fig. 8*C*). Thus, these results suggest that both inhibition of GSH synthesis and stimulation of GSH transport by MK571 are necessary for the induction of apoptosis.

DISCUSSION

Recent reports have discovered new roles for changes in the intracellular milieu during apoptosis (denominated permissive apoptotic environment) as determinants in the activation of the apoptotic machinery (5, 35, 71). Glutathione loss is a common feature during apoptosis induced by different stimuli, and it has been clearly demonstrated that GSH depletion in FasL-induced apoptosis is mediated by its efflux (21–23, 32). We previously demonstrated that GSH depletion is necessary for the activation of the execution phase of FasL-induced apoptosis (22), independent of the increases in ROS (34). However, the mechanisms by which GSH loss regulates cell death remain unclear. In this study we report that GSH efflux is tightly coupled to the progression of AVD and is necessary for the changes in ionic homeostasis during apoptosis. Moreover, we demonstrate that GSH loss regulates the progression of apoptosis by the modulation of K^+ loss, which further regulates the execution phase of apoptosis. Finally, we also show that apoptosis can be induced by both GSH synthesis inhibition and stimulation of GSH transport in the absence of any apoptotic stimuli.

During FasL-induced apoptosis, GSH loss seems to occur in two different stages, neither of which is associated with the loss of membrane integrity (22). Here we present evidence for the correlation of these two stages of GSH loss with AVD. Apoptotic volume decrease and changes in ionic homeostasis are common features of apoptosis induced by different stimuli (5, 36, 37, 39, 61, 63, 72, 73). We report that the reduction in GSH content was correlated with AVD measured by changes in forward scatter and electronic cell sizing. The first stage of reduction in GSH content was associated with a decrease in cell diameter by ~8–11% translated in a cell volume decrease of ~17–28%. Additionally, the second stage of GSH loss is correlated with a decrease in cell diameter of ~50–62% (an actual volume decrease of ~92–94%) and plasma membrane blebbing. Similar results were previously described in FasL- and UV light-induced Jurkat cell apoptosis, and during radiation-induced thymocyte cell death (41, 42, 74), where a two-stage AVD

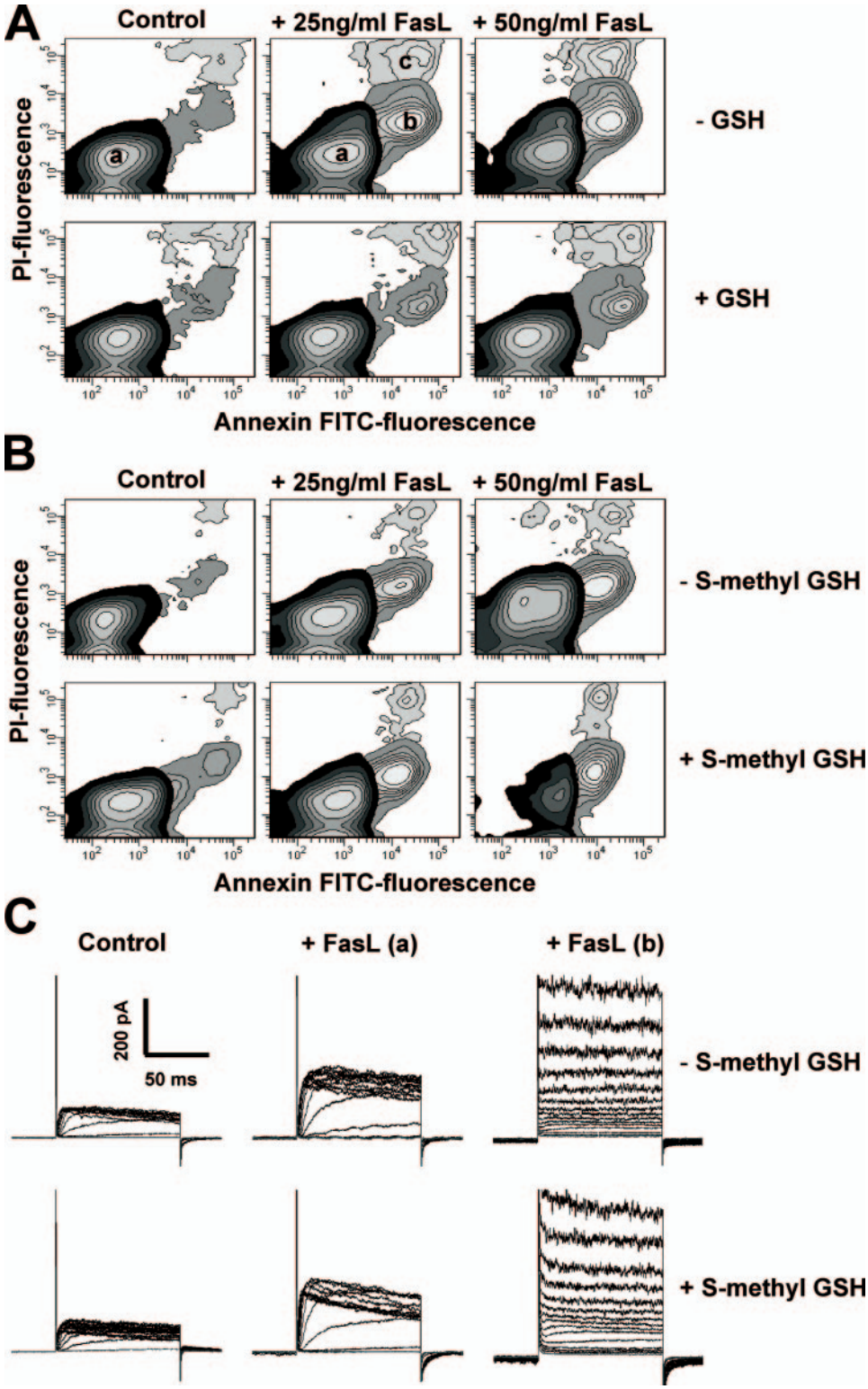

FIGURE 7. **The regulation of apoptosis and ionic conductances by GSH depends on the −SH (thiol) group.** FasL-induced apoptosis was assessed by phosphatidylserine externalization (annexin V binding) and loss of plasma membrane integrity or cell viability (PI). Apoptosis was induced by FasL during 4 h. The effect of high extracellular GSH (*A*) and *S*-methyl-GSH (25 mM) (*B*) was assessed. Externalization of phosphatidylserine is shown as an increase in the number of cells that had an increase in annexin V-FITC fluorescence (*population b*), prior to the loss of membrane integrity or high PI fluorescence with respect to control cells (*a*). Loss of plasma membrane integrity or cell viability in later stages of apoptosis is reflected as an increase in both PI and FITC fluorescence (*c*). The contour plots are representative of $n = 3$ independent experiments. *C,* activation of the ion channels by FasL was performed as in Fig. 4 in the presence or absence of *S*-methyl-GSH. FasL-induced increase in the amplitude of Kv1.3- (*a*) and ORCC-mediated currents (*b*) remained unaffected by the presence of *S*-methyl-GSH. *S*-Methyl-GSH did not prevent activation of ORCC and increase in Kv1.3 current amplitude (in 4 of 12 recordings in + *S*-methyl-GSH, compared with 4 of 11 recordings in *S*-methyl-GSH) induced by FasL. Plots in all cases are representatives of at least three independent experiments except for *FasL* (*a*) *panels,* where currents are representative of the population with increase Kv1.3 current amplitude, 36% (−*S*-methyl-GSH) and 33% (+*S*-methyl-GSH) of the recordings as in Fig. 4.

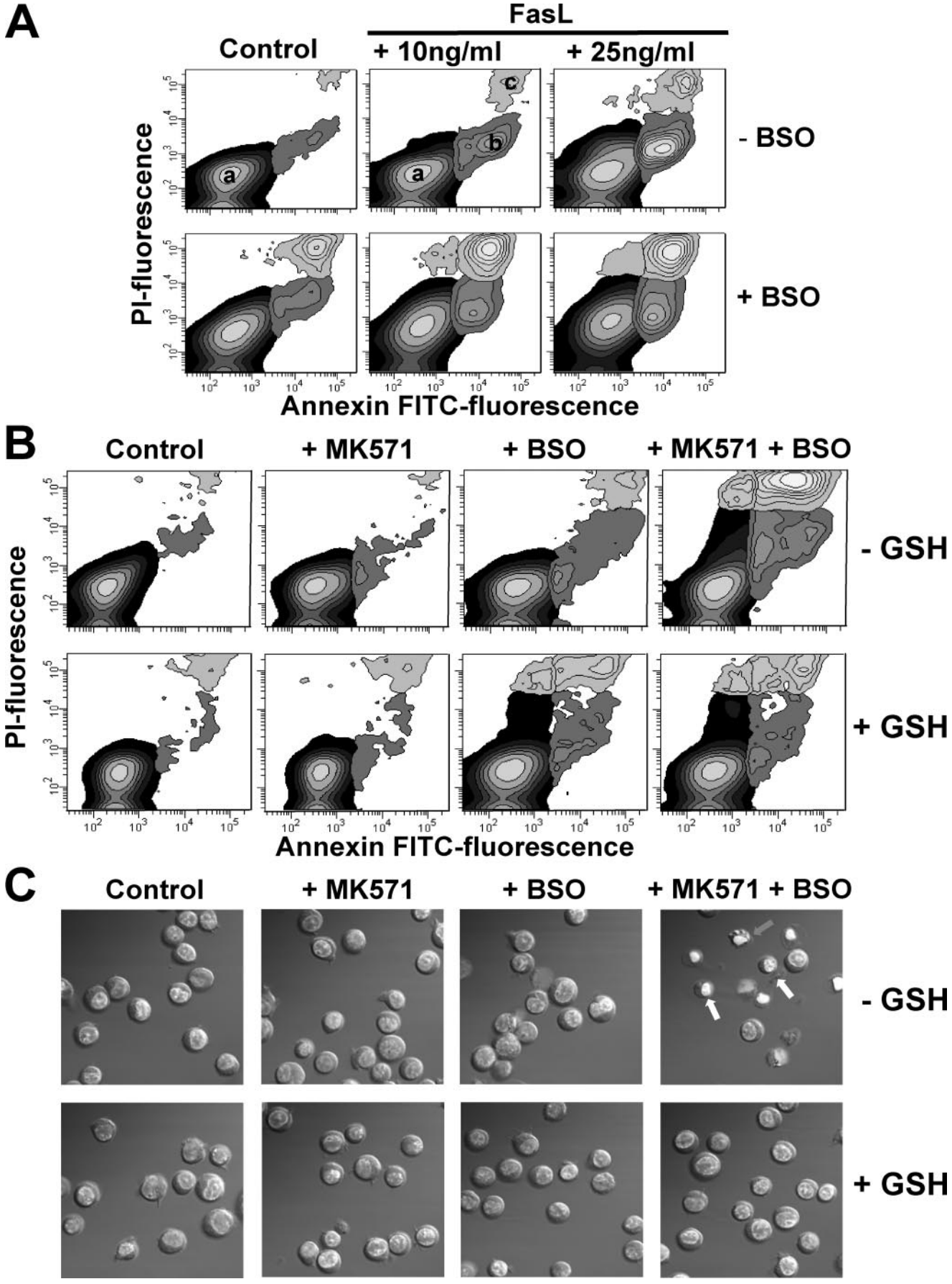
A
FasL
Control
+ 10ng/ml
+ 25ng/ml
- BSO
+ BSO
PI-fluorescence
Annexin FITC-fluorescence
a
b
c
B
Control
+ MK571
+ BSO
+ MK571 + BSO
- GSH
+ GSH
PI-fluorescence
Annexin FITC-fluorescence
C
Control
+ MK571
+ BSO
+ MK571 + BSO
- GSH
+ GSH

was reported with similar degrees of cell shrinkage for both stages.

Because AVD and changes in ionic homeostasis (particularly K^+ loss) also regulate the progression of apoptosis (5, 35, 39, 42, 51, 52, 60, 61, 63, 72, 73, 75–77), we explored the link between GSH depletion, changes in ionic homeostasis, and apoptosis. FasL induces the activation of ORCC; however, net Cl^- depletion does not occur during FasL-induced apoptosis, and thus, changes in intracellular Cl^- distribution do not participate in the progression of cell death (62). We focused then on the role of K^+ depletion in apoptotic cell death. Intracellular K^+ loss is necessary for the progression of apoptosis at different stages of the signaling cascade, including cytochrome *c* release, apoptosome formation, caspase and endonuclease activation (5, 51, 52, 60, 61, 63, 72, 75). The loss of GSH was shown to be necessary for the changes in ionic homeostasis to occur. High extracellular GSH prevented K^+ loss induced by FasL; conversely, stimulation of GSH efflux accelerated K^+ depletion. In addition, we observed that although GSH depletion is largely independent from K^+ loss, K^+ depletion is required for the progression of apoptosis and for its acceleration by MK571. These results suggest that GSH efflux modulates the progression of the execution phase of apoptosis at least in part by modulating K^+ loss during apoptosis. It is important to mention that although FasL induces Kv1.3 and ORCC activation, their inhibition by ShkDap22 and DIDS does not prevent the changes in ionic homeostasis and the progression of apoptosis (51, 62). Thus, other ionic pathways must be involved in both the ionic imbalance induced by Fas activation and the progression of cell death. T cells and lymphoma cells (including Jurkat cells) have been reported to have several types of K^+ channels, including calcium-activated (78) and voltage-activated K^+ channels (not shaker-related) (79), which might be involved in K^+ depletion during apoptosis. In addition, apoptosis is not only paralleled by changes in K^+ content but also by changes in intracellular Na^+ and plasma membrane depolarization, and these changes are associated with impairment of the Na^+-K^+-ATPase (73, 76, 80–82). Indeed, recent reports demonstrated that impairment in the Na^+-K^+-ATPase activity during apoptosis is also regulated by GSH depletion (76, 83).

The role of GSH in distinct cell processes, including apoptosis, has been mainly ascribed to its potent antioxidant properties. A wide variety of ion channels and transporters are regulated by ROS (37, 84, 85). Recent reports have shown that AVD and the activation of ion channels involved in the progression of apoptosis are modulated by ROS (37, 38). Furthermore, some studies have demonstrated inhibition of AVD and ion channels by extracellular thiols, but this was associated with ROS generation (37). We have shown that the regulation of apoptosis by changes in GSH content is independent from the excessive accumulation of ROS and oxidative stress (34). Thus other mechanisms distinct from ROS formation must be involved in the regulation of AVD and ionic homeostasis by GSH depletion.

Glutathione is freely distributed in the cytosol, reaching a concentration of up to 10 mM in some cells (8, 9), which suggests that its loss might contribute to the osmotic imbalance required for cell shrinkage during apoptosis. We demonstrate that the regulation of AVD by GSH depletion involves further modulation of ionic conductances. Glutathione is negatively charged at physiological pH within the cell (as a thiolate anion GS^-), which might suggest that GSH efflux acts as a counter ion for the major loss of cations and the concomitant cell shrinkage. Thus, it is likely that GSH loss is coupled to the changes in ionic homeostasis by its electrical charge. However, our previous studies suggest that GSH loss occurs through a GSH/organic anion (OA^-) exchange with characteristics of an *SLCO*/organic anion-transporting polypeptide, which has been shown to have a stoichiometry of 1(GSH) to 1(OA^-) (86–88). If this is true, then GSH loss should contribute neither to the osmotic imbalance that induces cell shrinkage nor as a counter ion for cation efflux during apoptosis. Glutathione depletion during apoptosis has been also suggested to be mediated by the ATP-dependent multidrug resistance proteins (*ABCC*/MRPs) (12, 16, 32, 89–91). In contrast, we and others have shown that inhibition of MRP transport accelerates the progression of apoptosis (22, 34, 92). Ballatori and co-workers (93) recently demonstrated that overexpression of MRP1 protects rather than stimulates Fas-induced apoptosis. It is clear then that further studies are required to clearly elucidate the molecular identity of the transporter(s) mediating GSH loss during apoptosis and the mechanisms regulating this process.

Glutathione depletion might have an indirect effect on AVD and ionic conductances. We also report here that the regulatory role of GSH on both apoptosis and the activation of ionic conductances still depends on its thiol group (−SH). Thiol/disulfide exchange reactions at the level of cysteine residues in proteins depend on the −SH group of GSH and have been suggested to regulate the progression of apoptosis (68, 94), Thiol-exchange reactions might also be involved in the regulation of ion channels and changes in the ionic homeostasis of the cell. In fact, previous reports demonstrate that sulfhydryl groups within cytosolic cysteine domains of ion channels directly modulate channel activity (95–97).

Apoptosis has been shown to induce both GSH depletion by its efflux (20–23, 32, 33, 65), and inhibition of its synthesis by caspase-mediated cleavage of the γ-glutamylcysteine synthetase (66, 67). Here we demonstrate that apoptosis can indeed be induced by both inhibition of its synthesis with BSO and activation of its efflux transport (with MK571) in the absence of any apoptotic stimuli. In conclusion, changes in intracellular GSH are required for the changes in ionic homeostasis that regulate

FIGURE 8. **GSH depletion induces apoptosis in the absence of an apoptotic stimuli.** Apoptosis was assessed by phosphatidylserine externalization (annexin V binding), loss of plasma membrane integrity or cell viability (PI) (*A* and *B*), and the appearance of morphological features such as cell shrinkage and nuclei condensation assessed by DIC optics (*C*). Cells were preincubated with BSO (200 μM, 24 h) and then treated with FasL or MK571 (50 μM) for 4 h in the presence or absence of high extracellular GSH (25 mM). Externalization of phosphatidylserine is shown as an increase in the number of cells that had an increase in annexin V-FITC fluorescence (*population b*), prior to the loss of membrane integrity or high PI fluorescence with respect to control cells (*a*). Loss of plasma membrane integrity or cell viability in later stages of apoptosis (also named late necrosis) is reflected as an increase in both PI and FITC fluorescence (*c*). The contour plots and images are representative of $n = 3$ independent experiments.

AVD and apoptosis. Moreover, GSH loss regulates the progression of the execution phase of apoptosis, at least in part, by modulation of K^+ loss. Finally, apoptosis can be induced by both GSH synthesis inhibition and stimulation of GSH transport in the absence of any apoptotic stimuli. Together, these results suggest that GSH depletion and K^+ loss are part of the permissive apoptotic environment required for the progression of the cell demise.

Acknowledgments—We acknowledge Dr. James W. Putney and Dr. David S. Miller for review of this manuscript. We also acknowledge Dr. Guillermo Vazquez (University of Toledo) for insight in the electrophysiology experiments. We appreciate Jeff Tucker for technical support in the confocal microscopy, and the NCI Fellows Editorial Board for its constructive comments on the manuscript.

REFERENCES

1. Green, D. R. (2003) *Immunol. Rev.* **193,** 5–9
2. Fadeel, B., and Orrenius, S. (2005) *J. Intern. Med.* **258,** 479–517
3. Brunner, T., Wasem, C., Torgler, R., Cima, I., Jakob, S., and Corazza, N. (2003) *Semin. Immunol.* **15,** 167–176
4. Hengartner, M. O. (2000) *Nature* **407,** 770–776
5. Bortner, C. D., and Cidlowski, J. A. (2004) *Pfluegers Arch.* **448,** 313–318
6. Wu, G., Fang, Y. Z., Yang, S., Lupton, J. R., and Turner, N. D. (2004) *J. Nutr.* **134,** 489–492
7. Schafer, F. Q., and Buettner, G. R. (2001) *Free Radic. Biol. Med.* **30,** 1191–1212
8. Franco, R., Schoneveld, O. J., Pappa, A., and Panayiotidis, M. I. (2007) *Arch. Physiol. Biochem.* **113,** 234–258
9. Forman, H. J., Zhang, H., and Rinna, A. (2008) *Mol. Aspects Med.* doi: 10.1016/j.mam.2008.08.006
10. Lu, S. C. (2008) *Mol. Aspects Med.* doi:10.1016/j.mam.2008.05.005
11. Merendino, N., Loppi, B., D'Aquino, M., Molinari, R., Pessina, G., Romano, C., and Velotti, F. (2005) *Nutr. Cancer* **52,** 225–233
12. Benlloch, M., Ortega, A., Ferrer, P., Segarra, R., Obrador, E., Asensi, M., Carretero, J., and Estrela, J. M. (2005) *J. Biol. Chem.* **280,** 6950–6959
13. Osbild, S., Brault, L., Battaglia, E., and Bagrel, D. (2006) *Anticancer Res.* **26,** 3595–3600
14. Circu, M. L., and Aw, T. Y. (2008) *Free Radic. Res.* **42,** 689–706
15. Hall, A. G. (1999) *Adv. Exp. Med. Biol.* **457,** 199–203
16. He, Y. Y., Huang, J. L., Ramirez, D. C., and Chignell, C. F. (2003) *J. Biol. Chem.* **278,** 8058–8064
17. Circu, M. L., Stringer, S., Rhoads, C. A., Moyer, M. P., and Aw, T. Y. (2008) *Biochem. Pharmacol.* doi:10.1016/j.bcp.2008.09.011
18. Oda, T., Sadakata, N., Komatsu, N., and Muramatsu, T. (1999) *J. Biochem.* (*Tokyo*) **126,** 715–721
19. Trompier, D., Chang, X. B., Barattin, R., du Moulinet D'Hardemare, A., Di Pietro, A., and Baubichon-Cortay, H. (2004) *Cancer Res.* **64,** 4950–4956
20. Hammond, C. L., Madejczyk, M. S., and Ballatori, N. (2004) *Toxicol. Appl. Pharmacol.* **195,** 12–22
21. Ghibelli, L., Fanelli, C., Rotilio, G., Lafavia, E., Coppola, S., Colussi, C., Civitareale, P., and Ciriolo, M. R. (1998) *FASEB J.* **12,** 479–486
22. Franco, R., and Cidlowski, J. A. (2006) *J. Biol. Chem.* **281,** 29542–29557
23. van den Dobbelsteen, D. J., Nobel, C. S., Schlegel, J., Cotgreave, I. A., Orrenius, S., and Slater, A. F. (1996) *J. Biol. Chem.* **271,** 15420–15427
24. Armstrong, J. S., and Jones, D. P. (2002) *FASEB J.* **16,** 1263–1265
25. Haouzi, D., Lekehal, M., Tinel, M., Vadrot, N., Caussanel, L., Letteron, P., Moreau, A., Feldmann, G., Fau, D., and Pessayre, D. (2001) *Hepatology* **33,** 1181–1188
26. Varghese, J., Khandre, N. S., and Sarin, A. (2003) *Apoptosis* **8,** 363–370
27. Sato, T., Machida, T., Takahashi, S., Iyama, S., Sato, Y., Kuribayashi, K., Takada, K., Oku, T., Kawano, Y., Okamoto, T., Takimoto, R., Matsunaga, T., Takayama, T., Takahashi, M., Kato, J., and Niitsu, Y. (2004) *J. Immunol.* **173,** 285–296
28. Friesen, C., Kiess, Y., and Debatin, K. M. (2004) *Cell Death Differ.* **11,** Suppl. 1, 73–85
29. Watson, R. W., Rotstein, O. D., Jimenez, M., Parodo, J., and Marshall, J. C. (1997) *Blood* **89,** 4175–4181
30. Kohno, T., Yamada, Y., Hata, T., Mori, H., Yamamura, M., Tomonaga, M., Urata, Y., Goto, S., and Kondo, T. (1996) *J. Immunol.* **156,** 4722–4728
31. Chiba, T., Takahashi, S., Sato, N., Ishii, S., and Kikuchi, K. (1996) *Eur. J. Immunol.* **26,** 1164–1169
32. Hammond, C. L., Marchan, R., Krance, S. M., and Ballatori, N. (2007) *J. Biol. Chem.* **282,** 14337–14347
33. Liuzzi, F., Fanelli, C., Ciriolo, M. R., Cerella, C., D'Alessio, M., Denicola, M., Magrini, A., Bergamaschi, A., and Ghibelli, L. (2003) *Ann. N. Y. Acad. Sci.* **1010,** 441–445
34. Franco, R., Panayiotidis, M. I., and Cidlowski, J. A. (2007) *J. Biol. Chem.* **282,** 30452–30465
35. Franco, R., Bortner, C. D., and Cidlowski, J. A. (2006) *J. Membr. Biol.* **209,** 43–58
36. Lang, F., Shumilina, E., Ritter, M., Gulbins, E., Vereninov, A., and Huber, S. M. (2006) *Contrib. Nephrol.* **152,** 142–160
37. Shimizu, T., Numata, T., and Okada, Y. (2004) *Proc. Natl. Acad. Sci. U. S. A.* **101,** 6770–6773
38. Reinehr, R., Becker, S., Eberle, A., Grether-Beck, S., and Haussinger, D. (2005) *J. Biol. Chem.* **280,** 27179–27194
39. Bortner, C. D., and Cidlowski, J. A. (2003) *J. Biol. Chem.* **278,** 39176–39184
40. Hedley, D. W., and Chow, S. (1994) *Cytometry* **15,** 349–358
41. Bortner, C. D., Sifre, M. I., and Cidlowski, J. A. (2007) *Methods Enzymol.* **428,** 161–181
42. Bortner, C. D., Sifre, M. I., and Cidlowski, J. A. (2008) *J. Biol. Chem.* **283,** 7219–7229
43. Bortner, C. D., and Cidlowski, J. A. (2002) *Cell Death Differ.* **9,** 1307–1310
44. Shiffer, Z., Zurgil, N., Shafran, Y., and Deutsch, M. (2001) *Biochem. Biophys. Res. Commun.* **289,** 1320–1327
45. Bortner, C. D., and Cidlowski, J. A. (2007) *Arch. Biochem. Biophys.* **462,** 176–188
46. Panayiotidis, M. I., Bortner, C. D., and Cidlowski, J. A. (2006) *Acta Physiol.* (*Oxf.*) **187,** 205–215
47. Okada, Y., Shimizu, T., Maeno, E., Tanabe, S., Wang, X., and Takahashi, N. (2006) *J. Membr. Biol.* **209,** 21–29
48. Burg, E. D., Remillard, C. V., and Yuan, J. X. (2006) *J. Membr. Biol.* **209,** 3–20
49. Patel, A. J., and Lazdunski, M. (2004) *Pfluegers Arch.* **448,** 261–273
50. Wang, Z. (2004) *Pfluegers Arch.* **448,** 274–286
51. Storey, N. M., Gomez-Angelats, M., Bortner, C. D., Armstrong, D. L., and Cidlowski, J. A. (2003) *J. Biol. Chem.* **278,** 33319–33326
52. Yu, S. P., Yeh, C. H., Sensi, S. L., Gwag, B. J., Canzoniero, L. M., Farhangrazi, Z. S., Ying, H. S., Tian, M., Dugan, L. L., and Choi, D. W. (1997) *Science* **278,** 114–117
53. Spencer, R. H., Chandy, K. G., and Gutman, G. A. (1993) *Biochem. Biophys. Res. Commun.* **191,** 201–206
54. Gutman, G. A., Chandy, K. G., Grissmer, S., Lazdunski, M., McKinnon, D., Pardo, L. A., Robertson, G. A., Rudy, B., Sanguinetti, M. C., Stuhmer, W., and Wang, X. (2005) *Pharmacol. Rev.* **57,** 473–508
55. Kalman, K., Pennington, M. W., Lanigan, M. D., Nguyen, A., Rauer, H., Mahnir, V., Paschetto, K., Kem, W. R., Grissmer, S., Gutman, G. A., Christian, E. P., Cahalan, M. D., Norton, R. S., and Chandy, K. G. (1998) *J. Biol. Chem.* **273,** 32697–32707
56. Szabo, I., Lepple-Wienhues, A., Kaba, K. N., Zoratti, M., Gulbins, E., and Lang, F. (1998) *Proc. Natl. Acad. Sci. U. S. A.* **95,** 6169–6174
57. Gulbins, E., Brenner, B., Schlottmann, K., Welsch, J., Heinle, H., Koppenhoefer, U., Linderkamp, O., Coggeshall, K. M., and Lang, F. (1996) *Immunology* **89,** 205–212
58. Szabo, I., Gulbins, E., Apfel, H., Zhang, X., Barth, P., Busch, A. E., Schlottmann, K., Pongs, O., and Lang, F. (1996) *J. Biol. Chem.* **271,** 20465–20469
59. Cui, Y., Konig, J., Nies, A. T., Pfannschmidt, M., Hergt, M., Franke, W. W., Alt, W., Moll, R., and Keppler, D. (2003) *Lab. Investig.* **83,** 527–538
60. Cain, K., Langlais, C., Sun, X. M., Brown, D. G., and Cohen, G. M. (2001) *J. Biol. Chem.* **276,** 41985–41990
61. Karki, P., Seong, C., Kim, J. E., Hur, K., Shin, S. Y., Lee, J. S., Cho, B., and

Park, I. S. (2007) *Cell Death Differ.* **14,** 2068–2075
62. Heimlich, G., and Cidlowski, J. A. (2006) *J. Biol. Chem.* **281,** 2232–2241
63. Bortner, C. D., Hughes, F. M., Jr., and Cidlowski, J. A. (1997) *J. Biol. Chem.* **272,** 32436–32442
64. Meister, A. (1995) *Methods Enzymol.* **251,** 3–7
65. Ghibelli, L., Coppola, S., Rotilio, G., Lafavia, E., Maresca, V., and Ciriolo, M. R. (1995) *Biochem. Biophys. Res. Commun.* **216,** 313–320
66. Franklin, C. C., Krejsa, C. M., Pierce, R. H., White, C. C., Fausto, N., and Kavanagh, T. J. (2002) *Am. J. Pathol.* **160,** 1887–1894
67. Franklin, C. C., Rosenfeld-Franklin, M. E., White, C., Kavanagh, T. J., and Fausto, N. (2003) *FASEB J.* **17,** 1535–1537
68. Deas, O., Dumont, C., Mollereau, B., Metivier, D., Pasquier, C., Bernard-Pomier, G., Hirsch, F., Charpentier, B., and Senik, A. (1997) *Int. Immunol.* **9,** 117–125
69. Armstrong, J. S., Steinauer, K. K., Hornung, B., Irish, J. M., Lecane, P., Birrell, G. W., Peehl, D. M., and Knox, S. J. (2002) *Cell Death Differ.* **9,** 252–263
70. Devadas, S., Hinshaw, J. A., Zaritskaya, L., and Williams, M. S. (2003) *Free Radic. Biol. Med.* **35,** 648–661
71. Pervaiz, S., and Clement, M. V. (2002) *Biochem. Biophys. Res. Commun.* **290,** 1145–1150
72. Dallaporta, B., Hirsch, T., Susin, S. A., Zamzami, N., Larochette, N., Brenner, C., Marzo, I., and Kroemer, G. (1998) *J. Immunol.* **160,** 5605–5615
73. Nobel, C. S., Aronson, J. K., van den Dobbelsteen, D. J., and Slater, A. F. (2000) *Apoptosis* **5,** 153–163
74. Klassen, N. V., Walker, P. R., Ross, C. K., Cygler, J., and Lach, B. (1993) *Int. J. Radiat. Biol.* **64,** 571–581
75. Thompson, G. J., Langlais, C., Cain, K., Conley, E. C., and Cohen, G. M. (2001) *Biochem. J.* **357,** 137–145
76. Yin, W., Cheng, W., Shen, W., Shu, L., Zhao, J., Zhang, J., and Hua, Z. C. (2007) *Leukemia* (*Basingstoke*) **21,** 1669–1678
77. Ernest, N. J., Habela, C. W., and Sontheimer, H. (2008) *J. Cell Sci.* **121,** 290–297
78. Fanger, C. M., Rauer, H., Neben, A. L., Miller, M. J., Rauer, H., Wulff, H., Rosa, J. C., Ganellin, C. R., Chandy, K. G., and Cahalan, M. D. (2001) *J. Biol. Chem.* **276,** 12249–12256
79. Smith, G. A., Tsui, H. W., Newell, E. W., Jiang, X., Zhu, X. P., Tsui, F. W., and Schlichter, L. C. (2002) *J. Biol. Chem.* **277,** 18528–18534
80. Bortner, C. D., Gomez-Angelats, M., and Cidlowski, J. A. (2001) *J. Biol. Chem.* **276,** 4304–4314
81. Yu, S. P. (2003) *Biochem. Pharmacol.* **66,** 1601–1609
82. Wang, X. Q., Xiao, A. Y., Sheline, C., Hyrc, K., Yang, A., Goldberg, M. P., Choi, D. W., and Yu, S. P. (2003) *J. Cell Sci.* **116,** 2099–2110
83. Gilbert, M., and Knox, S. (1997) *J. Cell. Physiol.* **171,** 299–304
84. Kourie, J. I. (1998) *Am. J. Physiol.* **275,** C1–C24
85. Jiao, J. D., Xu, C. Q., Yue, P., Dong, D. L., Li, Z., Du, Z. M., and Yang, B. F. (2006) *Biochem. Biophys. Res. Commun.* **340,** 277–285
86. Ballatori, N., Hammond, C. L., Cunningham, J. B., Krance, S. M., and Marchan, R. (2005) *Toxicol. Appl. Pharmacol.* **204,** 238–255
87. Hagenbuch, B., and Meier, P. J. (2004) *Pfluegers Arch.* **447,** 653–665
88. Marzolini, C., Tirona, R. G., and Kim, R. B. (2004) *Pharmacogenomics* **5,** 273–282
89. Fico, A., Manganelli, G., Cigliano, L., Bergamo, P., Abrescia, P., Franceschi, C., Martini, G., and Filosa, S. (2008) *Free Radic. Biol. Med.* **45,** 211–217
90. Mueller, C. F., Widder, J. D., McNally, J. S., McCann, L., Jones, D. P., and Harrison, D. G. (2005) *Circ. Res.* **97,** 637–644
91. Laberge, R. M., Karwatsky, J., Lincoln, M. C., Leimanis, M. L., and Georges, E. (2007) *Biochem. Pharmacol.* **73,** 1727–1737
92. Blokzijl, H., van Steenpaal, A., Vander Borght, S., Bok, L. I., Libbrecht, L., Tamminga, M., Geuken, M., Roskams, T. A., Dijkstra, G., Moshage, H., Jansen, P. L., and Faber, K. N. (2008) *J. Biol. Chem.* **284,**
93. Marchan, R., Hammond, C. L., and Ballatori, N. (2008) *Biochim. Biophys. Acta* **1778,** 2413–2420
94. Pan, S., and Berk, B. C. (2007) *Circ. Res.* **100,** 213–219
95. Rozanski, G. J., and Xu, Z. (2002) *J. Mol. Cell. Cardiol.* **34,** 1623–1632
96. Zeidner, G., Sadja, R., and Reuveny, E. (2001) *J. Biol. Chem.* **276,** 35564–35570
97. Cai, S., and Sauve, R. (1997) *J. Membr. Biol.* **158,** 147–158